

63₃-018
63₁-012

9

[REDACTED]

46 L 13

1115,5
NACA 63/1



CONFIDENTIAL
FILE

RESEARCH MEMORANDUM

for the

Bureau of Aeronautics, Navy Department

BOUNDARY-LAYER AND STALLING CHARACTERISTICS OF TWO SYMMETRICAL

NACA LOW-DRAG AIRFOIL SECTIONS

By George B. McCullough and Donald E. Gault

Ames Aeronautical Laboratory
Moffett Field, Calif.

CLASSIFIED DOCUMENT

This document contains classified information affecting the National Defense of the United States within the meaning of the Espionage Act, USC 5 and 32. Its transmission or the revelation of its contents in any manner to an unauthorized person is prohibited by law. Information so classified may be imparted only to persons in the military and naval Services of the United States, appropriate civilian officers and employees of the Federal Government who have a legitimate interest therein, and to United States citizens of known loyalty and discretion who of necessity must be informed thereof.



ENGINEERING DEPT. LIBRARY
CHANCE VOUGHT AIRCRAFT
STRATFORD, CONN.

NATIONAL ADVISORY COMMITTEE FOR AERONAUTICS

WASHINGTON

JAN 6 1947

CLASSIFICATION CHANGED TO Unclassified
BY AUTHORITY OF NASA Rulebook #122
ON 10/16/86 OF gpc

[REDACTED]

NATIONAL ADVISORY COMMITTEE FOR AERONAUTICS

RESEARCH MEMORANDUM

for the

Bureau of Aeronautics, Navy Department

BOUNDARY-LAYER AND STALLING CHARACTERISTICS OF TWO SYMMETRICAL
NACA LOW-DRAG AIRFOIL SECTIONS

By George B. McCullough and Donald E. Gault

SUMMARY

Two symmetrical airfoils, an NACA 63₃-018 and an NACA 63₁-012, were investigated for the purpose of determining their stalling and boundary-layer characteristics with a view toward the eventual application of this information to the problem of boundary-layer control. Force measurements, pressure distributions, tuft studies, and boundary-layer-profile measurements were made at a value of 5,800,000 Reynolds number. It was found that the 18-percent-thick airfoil stalled progressively from the trailing edge because of separation of the turbulent boundary layer. In contrast, the 12-percent-thick airfoil stalled abruptly from a separation of flow near the leading edge before the turbulent boundary layer became subject to separation. From this it was concluded that if high values of lift are to be obtained with thin, high-critical-speed sections by means of boundary-layer control, the work must be directed toward delaying the separation of flow near the leading edge. It was found that the presence of a nose flap on the 12-percent-thick section caused the airfoil to stall in a manner similar to that of

the 18-percent-thick section.

INTRODUCTION

The idea of artificially controlling the boundary layer of an airfoil by means of suction or pressure slots for the purpose of increasing the maximum lift or reducing the profile drag is not new. Considerable research in this field has been done both in this country and abroad, but to date little, if any, practical use has been made of the method, partly because of uncertainty as to its efficacy, and partly because the additional complications of design outweighed the advantages. Consequently, boundary-layer control has remained in the laboratory, the subject of sporadic experiments, and usually of such small scale as to render the results unconvincing.

Recent developments of airplane design, however, have produced renewed interest in the subject and have resulted in a re-examination of existing data. One contributing factor to the renewed interest is the trend toward thin airfoil sections in the design of high-speed airplanes. Suitable high-speed airfoil sections, unfortunately, are characterized by low maximum lift coefficients even when equipped with the most effective of flaps. This deficiency results in undesirably high airplane landing speeds. Since but little improvement is to be expected from further flap research, the quest for a more effective high-lift device must turn in other directions. A second factor favorable to boundary-layer control is the increasing use of the gas turbine or jet engine as aircraft power plants. The large volume of induced air and the high-capacity compressor required by

these engines suggest at once a source of suction without additional equipment, and with a minimum of complication to the aircraft structure.

The combination of these two factors would seem to point toward artificial boundary-layer control as a means of obtaining satisfactory landing speeds with modern high-speed aircraft. With this in mind, the current experiments were undertaken, not as a direct assault on the problem of boundary-layer control, but rather to furnish preliminary information toward that end. Accordingly, extensive data were obtained on the stalling and boundary-layer characteristics of two low-drag airfoil sections at subcritical speeds for a moderately large value of Reynolds number.

Given in the appendix is a brief discussion of the validity of the boundary-layer-shape parameter as a universal parameter describing the shape of all turbulent velocity profiles.

This investigation was conducted in the Ames 7- by 10-foot wind tunnel No. 1.

SYMBOLS

- b wing span, 6.802 feet
c wing chord, 5.000 feet
 c_l section lift coefficient (corrected for jet-boundary effect by the method of reference 1) (L/q_0S)
 $c_{Q\delta^*}$ section displacement flow coefficient $[(U/U_0)(\delta^*/c)]$
H boundary-layer-shape parameter (δ^*/θ)
L lift, pounds

- p_l local static pressure
- p_o free-stream static pressure
- P pressure coefficient $\left(\frac{p_l - p_o}{q_o} \right)$
- q_o free-stream dynamic pressure $\left(\frac{1}{2} \rho_o U_o^2 \right)$
- S wing area, 34.010 square feet
- u local velocity inside boundary layer
- U local velocity outside boundary layer
- U_o free-stream velocity
- x distance measured along airfoil chord line from leading edge
- y distance above airfoil surface measured perpendicular to
tangent to surface
- α_o section angle of attack (corrected for jet-boundary effect
by the method of reference 1), degrees
- δ total boundary-layer thickness
- δ_f plain- or split-flap deflection, degrees
- δ_{nf} nose-flap deflection, degrees
- δ^* boundary-layer-displacement thickness

$$\left[\int_0^{\delta} \left(1 - \frac{u}{U} \right) dy \right]$$

- θ boundary-layer-momentum thickness

$$\left[\int_0^{\delta} \frac{u}{U} \left(1 - \frac{u}{U} \right) dy \right]$$

- ρ_o free-stream mass density

MODELS AND TESTS

Two models, designed to the ordinates of the NACA 63₃-018 and 63₁-012 airfoils (table I), were constructed of laminated mahogany for these tests. Both models were of 5-foot chord and spanned the 7-foot dimension of the wind-tunnel jet. Each model was provided with 27.5 percent chord, plain and split flaps hinged about the chord line and lower surface, respectively. In addition, a 10-percent-chord nose flap was investigated on the NACA 63₁-012 section. Sketches of these three flaps are shown in figures 1 and 2. Photographs of the models installed in the wind tunnel are shown in figure 3.

Force measurements were obtained by means of the usual wind-tunnel balance system. The pressure-distribution measurements were obtained by means of flush-type orifices located along the midspan of the model and connected to multiple-tube manometers. No orifices were provided in the split flaps. All pressures were recorded photographically.

Tuft studies were made by observing the stall patterns as indicated by small threads glued to the surface of the models.

Boundary-layer-velocity profiles were obtained by surveying the boundary layer with rakes attached to the surface of the airfoil. Several sizes of rakes were used depending on the thickness of the boundary layer. Surveys were made from 90 percent chord to as far forward along the chord as it was practical to go with the smallest rake. The smallest rakes were made of

0.015-inch-outside-diameter steel hypodermic tubing flattened to 0.007 inch at the ends.

All tests were made at a dynamic pressure of 40 pounds per square foot which, for the 5-foot-chord models, corresponds to a Reynolds number of about 5,800,000.

RESULTS AND DISCUSSION

Lift Characteristics

The lift characteristics of the two airfoils, plotted as the variation of section lift coefficient with angle of attack, are presented in the figures listed in the following table:

Fig. no.	Airfoil section	Trailing-edge flap		Nose-flap deflection (deg)
		Type	Deflection (deg)	
4(a)	63 ₃ -018	plain	0 to 40	---
4(b)	do.	split	0 to 40	---
5(a)	63 ₁ -012	plain	0 to 40	---
5(b)	do.	split	0 to 40	---
5(c)	do.	plain	0	0, 75, 90, 105, 120
5(d)	do.	plain	40.0	do.

The maximum section lift coefficients measured and the increments of lift due to flap deflection are summarized as follows:

Airfoil section	Trailing-edge flap		Nose-flap deflection (deg)	α_o for $C_{l_{max}}$ (deg)	$c_{l_{max}}$	$\Delta c_{l_{max}}$
	Type	Deflection (deg)				
63 ₃ -018	Plain	0	---	14.7	1.38	---
do.	Plain	40	---	10.7	2.18	0.80
do.	Split	40	---	13.9	2.69	1.31
63 ₁ -012	Plain	0	---	13.7	1.38	---
do.	Plain	40	---	8.1	2.06	0.68
do.	Split	40	---	8.6	2.13	0.75
do.	Plain	0	105	18.9	1.77	0.39
do.	Plain	40	105	14.0	2.42	0.36 ^a
						1.04 ^b

a Due to nose flap only.

b Due to both flaps.

The greater effectiveness of the plain and split flaps with the thicker airfoil is apparent. No attempt was made to find the maximum section lift coefficients attainable by deflecting the plain and split flaps to their optimum deflection angles; instead, the maximum flap deflection was arbitrarily limited to 40°. It is possible that greater maximum lift coefficients could have been obtained by other flap configurations, but an intensive study of flap effectiveness was not the purpose of this investigation.

Pressure Distribution

Pressure-distribution data were obtained throughout the

angle-of-attack range for all the flap configurations tested. The bulk of these data precludes presentation in this report. However, some characteristic pressure distributions for 0° geometric angle of attack and the angle of attack corresponding to the maximum lift coefficient are presented in the following figures:

Fig. no.	Airfoil section	Trailing-edge flap		Nose-flap deflection (deg)
		Type	Deflection (deg)	
6(a)	63 ₃ -018	plain	0	---
6(b)	do.	plain	40	---
6(c)	do.	split	40	---
7(a)	63 ₁ -012	plain	0	---
7(b)	do.	plain	40	---
7(c)	do.	split	40	---
7(d)	do.	plain	0	105
7(e)	do.	plain	40	105

No pressure measurements were made over the split flaps nor over the lower surface of the nose flap. The pressures over the upper surface of the nose flap are plotted along the axis ahead of the normal leading edge of the airfoil and are continuous with the upper surface pressures over the body of the airfoil. In no case was the minimum pressure measured over the nose flap less than the minimum pressure measured over the body of the airfoil.

Tuft Studies

The stalling characteristics of the two models as indicated by the action of small tufts glued to the upper surface of the models were observed. The results of these observations in the form of graphs showing the chordwise progression of the stalled area with increasing angle of attack are presented in the following figures:

Fig. no.	Airfoil section	Trailing-edge flap		Nose-flap deflection (deg)
		Type	Deflection (deg)	
8(a)	63 ₃ -018	plain	0	---
8(b)	do.	plain	40	---
8(c)	do.	split	40	---
9(a)	63 ₁ -012	plain	0	---
9(b)	do.	plain	40	---
9(c)	do.	split	40	---
9(d)	do.	plain	0	105
9(e)	do.	plain	40	105

It will be noted that the NACA 63₃-018 airfoil stalled first at the trailing edge, the stalled area progressing forward with increasing angle of attack. The effect of this type of stall is shown by the droop of the lift curves presented in figure 4. In contrast, the NACA 63₁-012 airfoil stalled abruptly. All the tufts reversed direction instantaneously with but little warning in the form

of rough flow over the trailing portion of the airfoil. The stall was so violent that for reasons of safety no attempts were made to obtain data for angles of attack greater than those of maximum lift.

The plain flaps of both airfoils were completely stalled when deflected 40° at all positive angles of attack.

The effect of the nose flap on the NACA 63₁-012 airfoil was to lessen the suddenness of the stall. The airfoil with the nose flap deflected stalled from the trailing edge forward, but not so gradually as the thicker airfoil. The violence of the stall was reduced sufficiently to allow data to be obtained for angles of attack greater than those of maximum lift.

Boundary-Layer Characteristics

A complete presentation of data for all the boundary-layer-velocity profiles measured during the course of this investigation is impractical because of its bulk; hence only a few representative profiles are presented in figures 10 and 11. However, the derived boundary-layer parameters, momentum thickness θ and shape parameter H are presented in their entirety for all configurations of the two airfoils investigated. These data, plotted as the variations of θ and H along the chord for various constant geometric angles of attack from 0° to the stall, are shown in the following listed figures:

Fig. no.	Airfoil section	Trailing-edge flap		Nose-flap deflection (deg)
		Type	Deflection (deg)	
12(a)	63 ₃ -018	plain	0	---
12(b)	do.	plain	40	---
12(c)	do.	split	40	---
13(a)	63 ₁ -012	plain	0	---
13(b)	do.	plain	40	---
13(c)	do.	split	40	---
13(d)	do.	plain	0	105
13(e)	do.	plain	40	105

Although many profiles of the laminar type were measured, the parameters θ and H were computed only for fully developed turbulent boundary layers. The integrations necessary to obtain θ and H were performed by mechanical methods. The discontinuities in the curves just behind the 0.7-chord station are believed to be the result of leakage of air through the flap nose gap.

von Doenhoff and Tetervin (reference 2) have shown that separation of the turbulent boundary layer has occurred when the shape parameter attains a value of 2.6. The National Bureau of Standards (reference 3) found this value to be 2.7. Inspection of the curves showing the variation of H along the chord of the NACA 63₃-018 airfoil (figs. 12(a), 12(b), and 12(c) indicates that large values of the shape parameter are attained over the after portion of the airfoil at high angles of attack. It is evident

that the stall of the airfoil originated from a turbulent separation which started at the trailing edge and moved steadily forward with increasing angle of attack. This type of stall pattern is characteristic of the thicker airfoils and has been frequently observed in the past. The chordwise locations of the turbulent separation points determined by extrapolating the shape-parameter data to a value of 2.6 agree well with the results of the tuft studies and pressure-distribution measurements. This gives further basis for acceptance of 2.6 as the critical value of the shape parameter indicative of separation of the turbulent boundary layer.

In contrast to the behavior of the 18-percent-thick section, the NACA 63₁-012 airfoil without nose flap stalled abruptly over the entire surface with only a slight warning indicated by rough flow over the after portion of the airfoil. Inspection of the shape-parameter data (figs. 13(a), 13(b), and 13(c)) shows that in no case, even with the curves extrapolated to the trailing edge, does the shape parameter approach the critical value of 2.6. Thus it is apparent that this moderately thin airfoil did not stall because of separation of the turbulent boundary layer, and it is surmised that the complete breakdown of flow resulted from the failure of a separated laminar boundary layer near the leading edge to reattach itself to the surface farther downstream.

It was thought that a short region of laminar separated flow might exist for angles of attack below that for the complete flow breakdown. Accordingly, attempts were made to measure the boundary layer along the upper surface forward to the leading edge, but

because of the thinness of the boundary layer and the physical limitations of the survey rake, it was impossible to obtain velocity profiles in the immediate vicinity of the leading edge. However, surveys made with a single total-head tube on the surface and a static tube slightly above the surface gave continuous readings up to zero percent chord, yielding no indication of the presence of a separated laminar boundary layer for angles of attack less than that corresponding to the stall.

Although no region of laminar separation was found in the immediate vicinity of the leading edge at angles of attack just below the stall, it is believed that the abrupt stall exhibited by moderately thin airfoils is due to the effect of small nose radii in promoting separation of the laminar boundary layers. For the present investigation it is thought that a laminar-type separation occurred on the lower surface of the nose radius, the position of the most rapid flow accelerations about the airfoil. Substantiation for this belief is given by the nose-flap data (figs. 13(d) and 13(e)). The presence of the nose flap so altered the boundary-layer-flow characteristics that turbulent separation occurred at the trailing edge prior to the complete stalling of the airfoil. The forward progress of the stalled area was more rapid than for the 18-percent-thick airfoil, but nevertheless the abruptness and violence of the stall were greatly reduced as compared to that of the 12-percent-thick airfoil without nose flap.

Two important considerations for the practical applications of artificial control of the boundary layer of an airfoil are the

chordwise locations of the slots and the blower capacity required. Previous investigations have shown that for the attainment of a given lift coefficient, suction control is more economical of power than the use of pressure slots or jets. (See references 4 and 5.) Consequently, only the use of suction slots will be considered in this discussion.

The results of references 6 and 7 have shown that suction slots operate near their maximum effectiveness when the quantity of air removed from the boundary layer is equal to that which would flow with a velocity equal to the local velocity outside of the boundary layer through an area of unit width and a height equal to the displacement thickness of the boundary layer. A section flow coefficient $c_{Q\delta^*} = \frac{U}{U_0} \frac{\delta^*}{C}$, which expresses this desired quantity of flow and is referred to in this report as the displacement-flow coefficient, was computed for both the airfoils investigated. Curves of the computed values of $c_{Q\delta^*}$ along the chords are presented in the following figures:

Fig. no.	Airfoil section	Trailing-edge flap		Nose-flap deflection (deg)
		Type	Deflection (deg)	
14(a)	63 ₃ -018	plain	0	---
14(b)	do.	plain	40	---
14(c)	do.	split	40	---
15(c)	63 ₁ -012	plain	0	---
15(b)	do.	plain	40	---
15(c)	do.	split	40	---
15(d)	do.	plain	0	105
15(e)	do.	plain	40	105

Insofar as the volume flow is concerned, the advantage of placing the suction slots well forward along the chord is apparent. What is not evident from these figures is the suction power required. At high angles of attack a forward location of the slot would require the blower to pump from a region of low pressure, thus requiring a greater expenditure of power per unit volume of air removed from the boundary layer. However, if the source of suction is assumed to be the compressor of a gas turbine or jet engine used normally to furnish the propulsive power of the aircraft, the relatively small amount of suction power required for boundary-layer control during the landing approach would not seem to be significant.

The effect of deflecting the plain or split flap on either

airfoil is to reduce markedly the thickness of the boundary layer for a given lift coefficient, thus reducing the suction volume required. This can be explained by the fact that the airfoils with flaps deflected possess an effectively less adverse pressure gradient opposing the boundary-layer flow because of larger negative pressures over the after portion of the airfoil body and flap.

When the application of artificial boundary-layer control to these two airfoils is considered, it would seem futile to locate suction slots along the afterbody of the NACA 63₁-012 airfoil if the stall results from laminar separation near the leading edge as is surmised from the evidence of this investigation. In contrast, consideration of the stalling characteristics of the NACA 63₃-018 airfoil section, which experienced turbulent separation from the trailing edge forward to about 60 percent chord at maximum lift, would indicate that suction slots located near the midchord should serve to delay turbulent separation to higher values of lift than is possible with the plain wing.

It should be mentioned that there is experimental evidence indicating that the 18-percent-thick airfoil stalls in a manner similar to the 12-percent section when the maximum lift is increased by the boundary-layer suction. Quinn (references 6 and 7) maintained flow about two 18-percent-thick airfoils by boundary-layer control beyond that obtainable with the plain sections until separation, believed laminar, occurred at the leading edges. It appears, then, that any airfoil of reasonable

thickness is subject to laminar separation at the leading edge; control of the turbulent boundary layer serves only to prolong steady flow about an airfoil until the critical conditions which cause laminar separation are reached at the leading edge.

The conditions leading to and causing separation and transition from a laminar-type flow to a turbulent flow have been the subject of considerable investigation, but theory and experiment are not sufficiently advanced for a complete understanding of the failure of a separated laminar boundary layer to reattach itself either as a laminar or turbulent boundary layer. The suddenness and violence of a stall originating from laminar separation precludes the practical application of an airfoil subject to its occurrence. Hence, if the full advantages of boundary-layer control are to be realized in the future, it would seem that a more thorough understanding of the laminar-separation phenomena is needed. This fact is emphasized by the present trend toward the use of thin, high-critical-speed airfoils which are more susceptible to laminar separation than are thicker sections.

However, any attempt to obtain increased maximum lift from thin airfoils should be directed towards the prevention of laminar separation in the vicinity of the leading edge. Two possible methods are suggested:

1. To decrease the effective angle of attack at the leading edge by means of a nose flap similar to the one used in this investigation or by use of a hinged nose section (drop-nose flap).
2. The use of a boundary-layer suction slot at or near the

point of separation.

Both methods would, of necessity, add to the structural complexity and weight of the wing and introduce the danger of spoiling the laminar-flow properties of the airfoil at its high-speed attitudes. The last method seems to offer the least complications to the wing structure, provided, of course, a source of suction is already available and the only additional design feature required is the necessary ducting to put it into use. The effectiveness of suction slots for controlling laminar separation near the leading edge, however, still lacks experimental confirmation, and further research is necessary before practical applications can be made.

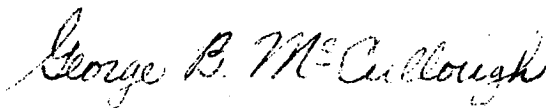
CONCLUDING REMARKS

The investigation of the stalling and boundary-layer characteristics of the two airfoil sections reported herein disclosed two different types of stalls: (1) a steady and progressive stall starting with the separation of the turbulent boundary layer at the trailing edge, and (2) an abrupt and complete separation of flow originating at the leading edge.

It has been demonstrated in the past that separation of the turbulent layer can be delayed by means of suction slots to higher values of lift than are attainable with the plain airfoil. However, the results of two recent investigations showed that this type of control served only to delay turbulent separation until critical conditions are reached which precipitate laminar

separation of flow in the vicinity of the leading edge. For practical applications of boundary-layer control, obtaining maximum increases in lift would seem, therefore, to depend on delaying not only the turbulent separation, as has been done in the past, but also the leading-edge separation. Furthermore, if both types of flow separation are to be delayed, the sequence of applying boundary-layer control would be reversed for thick and thin airfoils. Although the leading-edge type of flow failure was satisfactorily delayed in the current investigation by the installation of a nose flap, it should be noted that there is no experimental evidence indicating that boundary-layer control by suction will successfully forestall this type of flow separation. Further research on this problem is indicated before the full benefits of boundary-layer control can be realized.

Ames Aeronautical Laboratory,
National Advisory Committee for Aeronautics,
Moffett Field, Calif.



George B. McCullough,
Aeronautical Engineer.




Donald E. Gault,
Aeronautical Engineer.

Approved:



Donald H. Wood,
Aeronautical Engineer.



APPENDIX

COMPARISON OF SHAPE PARAMETERS

Although the primary purpose of this investigation was to obtain information which would be of value in boundary-layer-control problems, the data are equally applicable to the study of the mechanics of turbulent separation. The incidental relevance of this second problem did not warrant a detailed analysis, but some information is given herein which is believed to be of sufficient interest to merit inclusion in this report.

A recent publication dealing with turbulent separation is the work of von Doenhoff and Tetervin (reference 2), in which is derived an empirical method of predicting the occurrence of turbulent separation on airfoils and bodies of revolution. A fundamental assumption upon which their work is based is that the shape parameter H defines the shape of all turbulent-boundary-layer velocity profiles, justification being given from numerous boundary-layer data by the fact that all points of u/U plotted against H for a constant value of y/θ fall on a single curve.

A similar analysis given in reference 3, and although these data are consistent within themselves, systematic differences were found with the data of reference 2. The conclusion is drawn that H is not a universal parameter defining the shape of turbulent boundary layers for all flow conditions, but that the Reynolds number and condition of the model surface are modifying factors. Figure 16 presents the data of this investigation in a similar manner, and

substantiates the validity of H as a shape parameter insofar as these data are concerned. The curves of u/U plotted against H agree well with those of reference 3 except at the inner and outer extremities of the boundary layer. These differences may be ascribed, in part, to difference in the technique of obtaining the boundary-layer profiles. The exact shape of the boundary-layer profile near the surface, and the value of δ , the total boundary-layer thickness, are particularly difficult to determine.

It is interesting to note that if the parameter H is accepted as defining all turbulent-boundary-layer velocity profiles, then the values of the quantities δ^*/δ and θ/δ are fixed for any given value of H . Figure 17 presents these relationships as found for the present investigation in comparison with those of references 2 and 3. The exact shape of these curves depends considerably on the manner of fairing the boundary-layer data, and final judgment on the validity of H as a universal parameter defining the shape of all turbulent boundary layers should be reserved pending the accumulation of more boundary-layer data or the development of more precise means of measuring velocity profiles.

REFERENCES

1. Allen, H. Julian, and Vincenti, Walter G.: Wall Interference in a Two-Dimensional Flow Wind Tunnel with Consideration of the Effect of Compressibility. NACA ARR No. 4KO3, 1944.
2. von Doenhoff, Albert E., and Tetervin, Neal: Determination of General Relations for the Behavior of Turbulent Boundary Layers. NACA ACR No. 3G13, 1943.
3. Anon: Investigation of Separation of the Turbulent Boundary Layer (NACA Research Authorization S44-1) National Bureau of Standards Progress Report, May 17, 1944.
4. Bamber, Millard J.: Wind Tunnel Tests on Airfoil Boundary Layer Control Using a Backward-Opening Slot. NACA Rep. No. 385, 1931.
5. Freeman, Hugh B.: Boundary-Layer-Control Tests of Two Wings in the Langley Propeller-Research Tunnel. NACA TN No. 1007, 1946.
6. Quinn, John H., Jr.: Tests of the NACA 63₃-018 Airfoil Section with Boundary-Layer Control by Suction. NACA CB No. L4H10, 1944.
7. Quinn, John H., Jr.: Wind-Tunnel Investigation of Boundary-Layer Control By Suction on the NACA 65₃-418, $\alpha = 1.0$ Airfoil-Section with a 0.29 Airfoil-Chord Double-Slotted Flap. NACA MR No. L5J05, 1945.

TABLE I.- ORDINATES FOR NACA 63₃-018 AND 63₁-012
AIRFOIL SECTIONS

Station percent chord	63 ₃ -018	63 ₁ -012
	Ordinate percent chord	Ordinate percent chord
0	0	0
.5	1.404	.985
.75	1.713	1.194
1.25	2.717	1.519
2.5	3.104	2.102
5	4.362	2.925
7.5	5.308	3.542
10	6.068	4.039
15	7.225	4.799
20	8.048	5.342
25	8.600	5.712
30	8.913	5.930
35	9.000	6.000
40	8.845	5.920
45	8.482	5.704
50	7.942	5.370
55	7.256	4.935
60	6.455	4.420
65	5.567	3.840
70	4.622	3.210
75	3.650	2.556
80	2.691	1.902
85	1.787	1.274
90	.985	.707
95	.348	.250
100	0	0

Leading-edge radius percent chord: 2.120 for the 63₃-018 airfoil section; 1.087 for the 63₁-012 airfoil section.

FIGURE LEGENDS

- Figure 1.- Sketches of the plain and split flaps used on the NACA 63₃-018 and NACA 63₁-012 airfoil sections.
- Figure 2.- Sketch of the nose flap used on the NACA 63₁-012 airfoil section.
- Figure 3.- Photographs of the two NACA 63-series airfoils mounted in the wind tunnel. (a) NACA 63₃-018 airfoil with plain flap deflected 40°. (b) NACA 63₁-012 airfoil with split flap deflected 40°.
- Figure 4.- Variation of the section lift coefficient with section angle of attack for the NACA 63₃-018 airfoil. (a) Plain flap deflected.
- Figure 4.- Concluded. (b) Split flap deflected.
- Figure 5.- Variation of the section lift coefficient with section angle of attack for the NACA 63₁-012 airfoil. (a) Plain flap deflected.
- Figure 5.- Continued. (b) Split flap deflected.
- Figure 5.- Continued. (c) Nose flap deflected.
- Figure 5.- Concluded. (d) Nose flap deflected; plain flap deflected 40°.
- Figure 6.- Pressure distribution over the NACA 63₃-018 airfoil. (a) Plain flap undeflected.
- Figure 6.- Continued. (b) Plain flap deflected 40°.
- Figure 6.- Concluded. (c) Split flap deflected 40°.
- Figure 7.- Pressure distribution over the NACA 63₁-012 airfoil. (a) Plain flap undeflected.
- Figure 7.- Continued. (b) Plain flap deflected 40°.
- Figure 7.- Continued. (c) Split flap deflected 40°.
- Figure 7.- Continued. (d) Nose flap deflected 105°.
- Figure 7.- Concluded. (e) Nose flap deflected 105°; plain flap deflected 40°.

Figure 8.- Stalling characteristics of the NACA 63₃-018 airfoil as indicated by tuft studies.

Figure 9.- Stalling characteristics of the NACA 63₁-012 airfoil as indicated by tuft studies. (a) Plain airfoil. (b) Plain flap 40°. (c) Split flap 40°.

Figure 9.- Concluded. (d) Nose flap 105°, plain flap 0°. (e) Nose flap 105°, plain flap 40°.

Figure 10.- Boundary-layer velocity profiles for the NACA 63₃-018 airfoil. (a) Plain flap, $\delta_f = 0^\circ$, 90 percent chord.

Figure 10.- Continued. (b) Plain flap, $\delta_f = 40^\circ$, 70 percent chord.

Figure 10.- Concluded. (c) Split flap, $\delta_f = 40^\circ$, 50 percent chord.

Figure 11.- Boundary-layer velocity profiles for the NACA 63₁-012 airfoil. (a) Plain flap, $\delta_f = 0^\circ$, 45 percent chord.

Figure 11.- Continued. (b) Plain flap, $\delta_f = 40^\circ$, 45 percent chord.

Figure 11.- Continued. (c) Split flap, $\delta_f = 40^\circ$, 90 percent chord.

Figure 11.- Continued. (d) Nose flap $\delta_{nf} = 105^\circ$, plain flap, $\delta_f = 0^\circ$, 60 percent chord.

Figure 11.- Concluded. (e) Nose flap, $\delta_{nf} = 105^\circ$, plain flap $\delta_f = 40^\circ$, 60 percent chord.

Figure 12.- Variation of the boundary-layer momentum thickness and shape parameter along the surface of the NACA 63₃-018 airfoil. (a) Plain flap, $\delta_f = 0^\circ$.

Figure 12.- Continued. (b) Plain flap, $\delta_f = 40^\circ$.

Figure 12.- Concluded. (c) Split flap, $\delta_f = 40^\circ$.

Figure 13.- Variation of the boundary-layer momentum thickness and shape parameter along the surface of the NACA 63₁-012 airfoil. (a) Plain flap, $\delta_f = 0^\circ$.

Figure 13.- Continued. (b) Plain flap, $\delta_f = 40^\circ$.

Figure 13.- Continued. (c) Split flap, $\delta_f = 40^\circ$.

Figure 13.- Continued. (d) Plain flap, $\delta_f = 0^\circ$. Nose flap, $\delta_{nf} = 105^\circ$.

Figure 13.- Concluded. (e) Plain flap, $\delta_f = 40^\circ$. Nose flap, $\delta_{nf} = 105^\circ$.

Figure 14.- Variation of the displacement flow coefficient along the surface of the NACA 63₃-018 airfoil. (a) Plain flap undeflected.

Figure 14.- Continued. (b) Plain flap deflected 40°.

Figure 14.- Concluded. (c) Split flap deflected 40°.

Figure 15.- Variation of the displacement flow coefficient along the surface of the NACA 63₁-012 airfoil. (a) Plain flap undeflected.

Figure 15.- Continued. (b) Plain flap deflected 40°.


Figure 15.- Continued. (c) Split flap deflected 40°.

Figure 15.- Continued. (d) Nose flap deflected 105°.

Figure 15.- Concluded. (e) Nose flap deflected 105°, plain flap deflected 40°.

Figure 16.- Variation of u/U with shape parameter for various values of y/θ .

Figure 17.- Comparison of the variations of δ^*/δ and θ/δ with shape parameter.



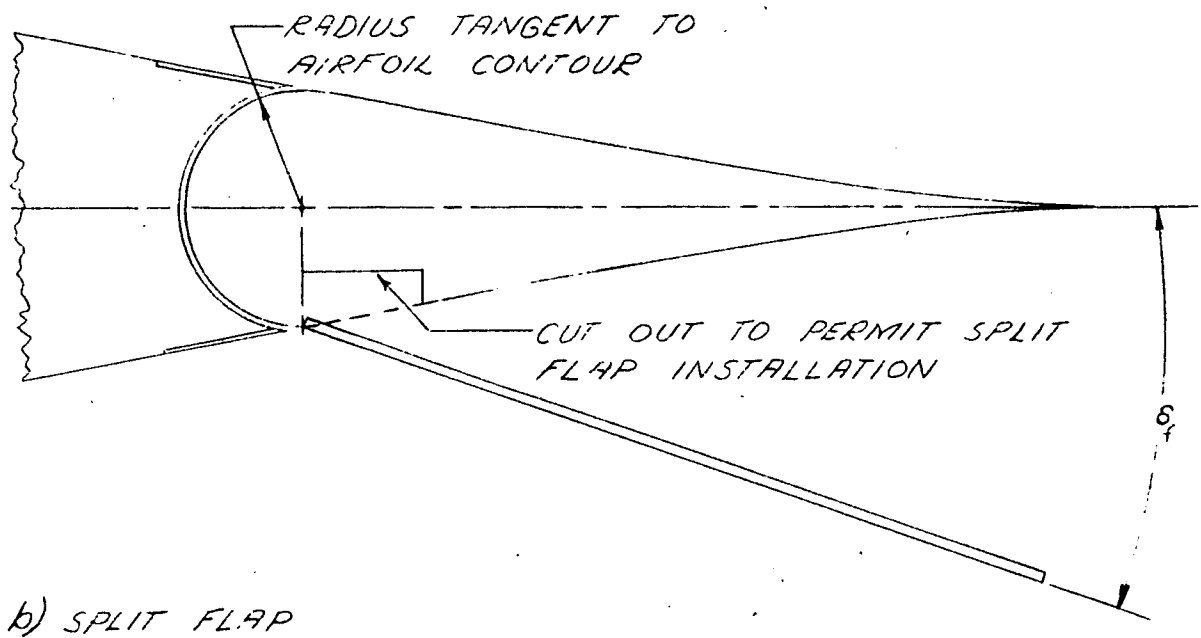
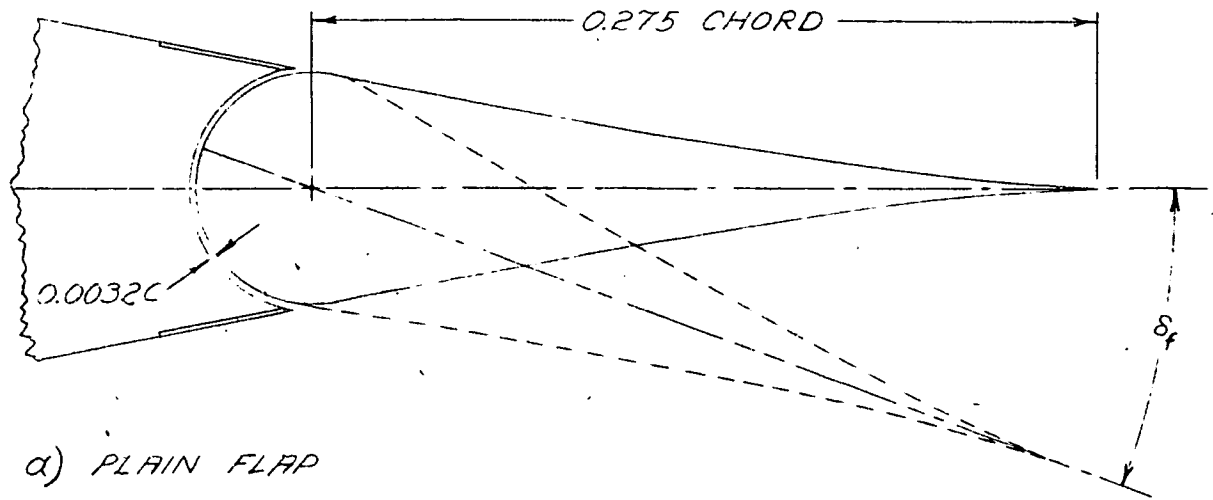


FIGURE 1 .- SKETCHES OF THE PLAIN AND SPLIT FLAPS USED ON THE NACA 63₃-018 AND NACA 63₁-012 AIRFOIL SECTIONS.

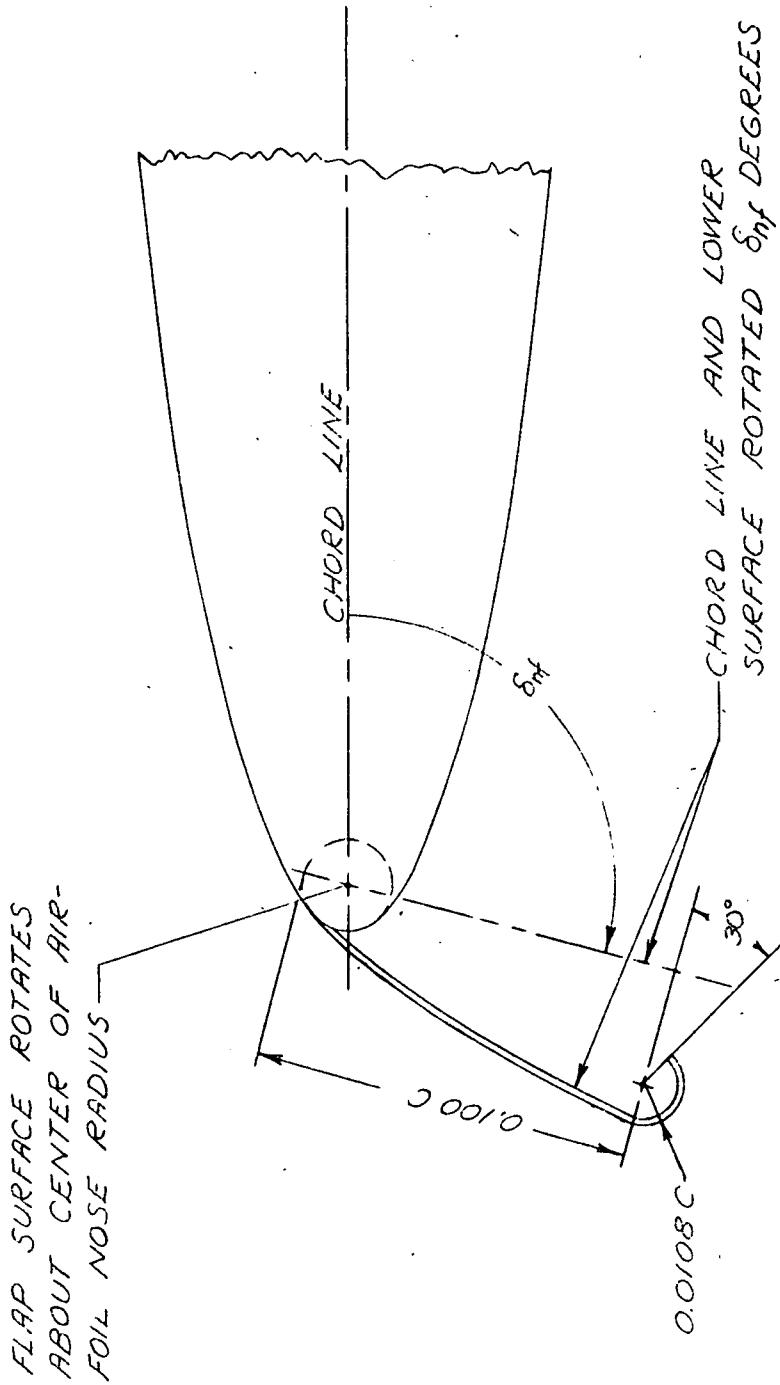


FIGURE 2. - SKETCH OF THE NOSE FLAP USED ON THE NACA 63-012 AIRFOIL SECTION.



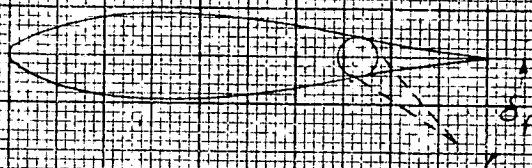
(a) NACA 633-018 airfoil with plain flap deflected 40° .



(b) NACA 631-012 airfoil with split flap deflected 40° .

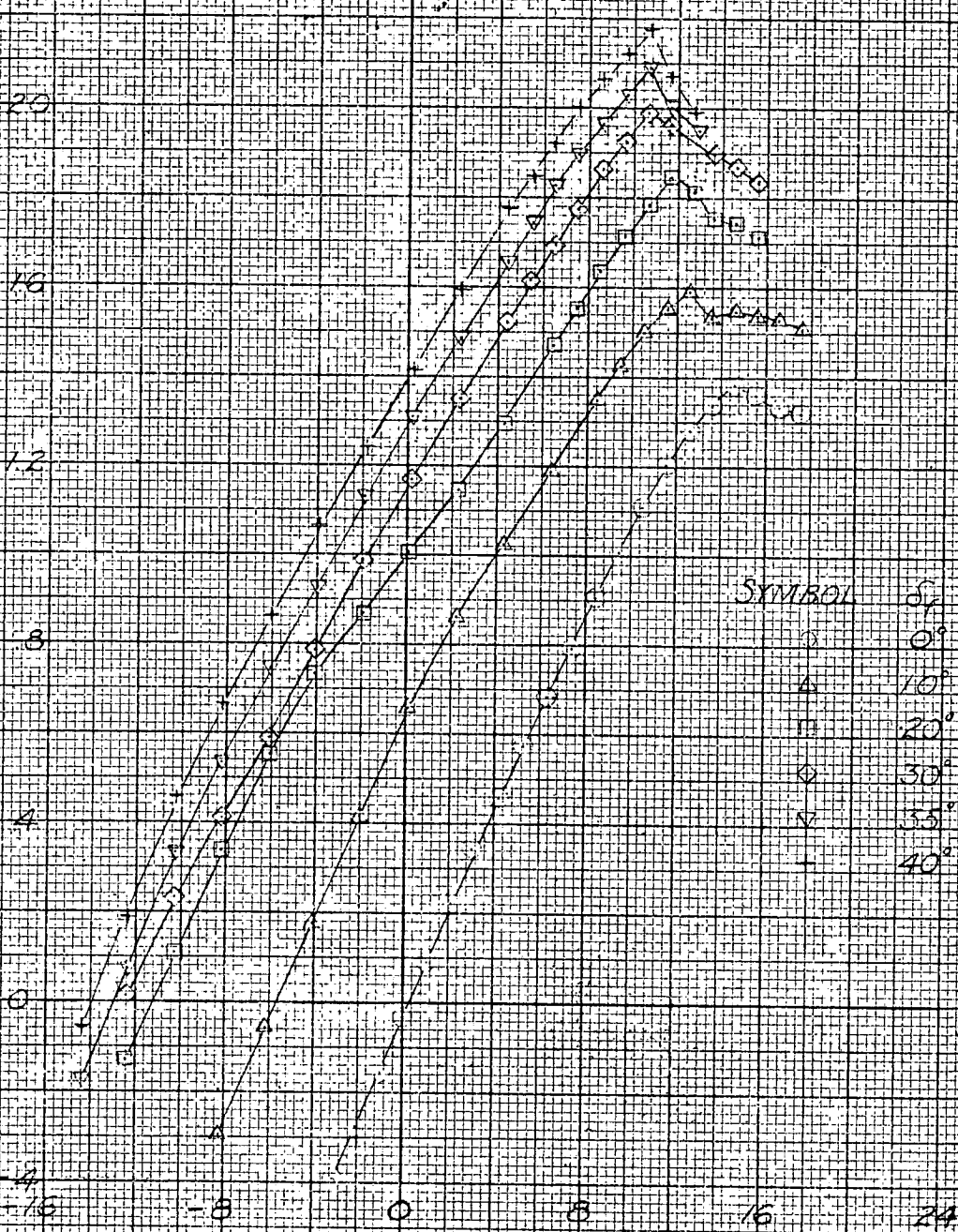
Figure 3.— Photographs of the two NACA 63-series airfoils mounted in the wind tunnel.

N.A.C.A. PHOTOGRAPH
NOT FOR PUBLICATION
UNLESS AUTHORIZED BY
NATIONAL ADVISORY COMMITTEE
FOR AERONAUTICS, WASHINGTON, D. C.



SECTION LIFT COEFFICIENT, C_l

24
20
16
12
8
4
0
-4
-8
-16

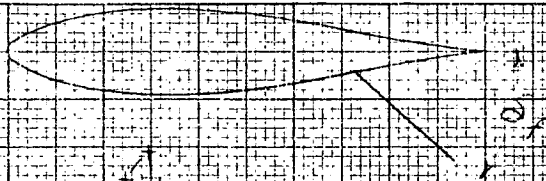


SYMBOL	δ_f
○	0°
△	10°
□	20°
◇	30°
▽	35°
+	40°

SECTION ANGLE OF ATTACK, α , DEG

(C) FLAP DEFLECTED.

FIGURE 4. VARIATION OF THE SECTION LIFT COEFFICIENT WITH SECTION ANGLE OF ATTACK FOR THE NACA 63-018 AIRFOIL.



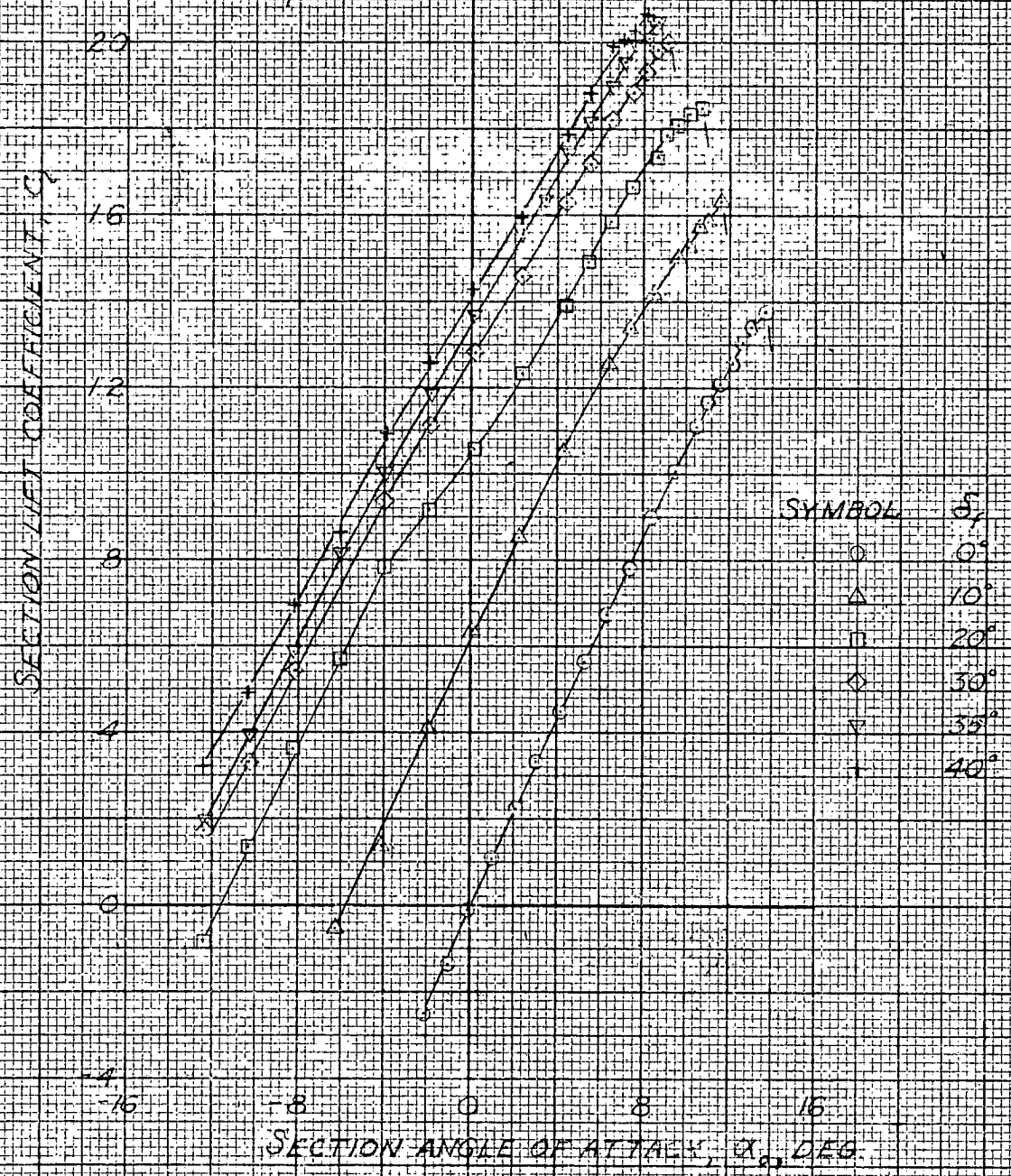
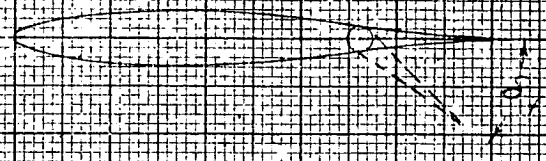
SECTION LIFT COEFFICIENT, C_L

28
24
20
16
12
8
4
0
-4

SECTION ANGLE OF ATTACK α_o , DEG.

SYMBOL	δ_f
○	RETRACTED
△	10°
□	20°
◇	30°
▽	35°
—	40°

(b) SPLIT FLAP TESTED
FIGURE 4 - CONCLUDED

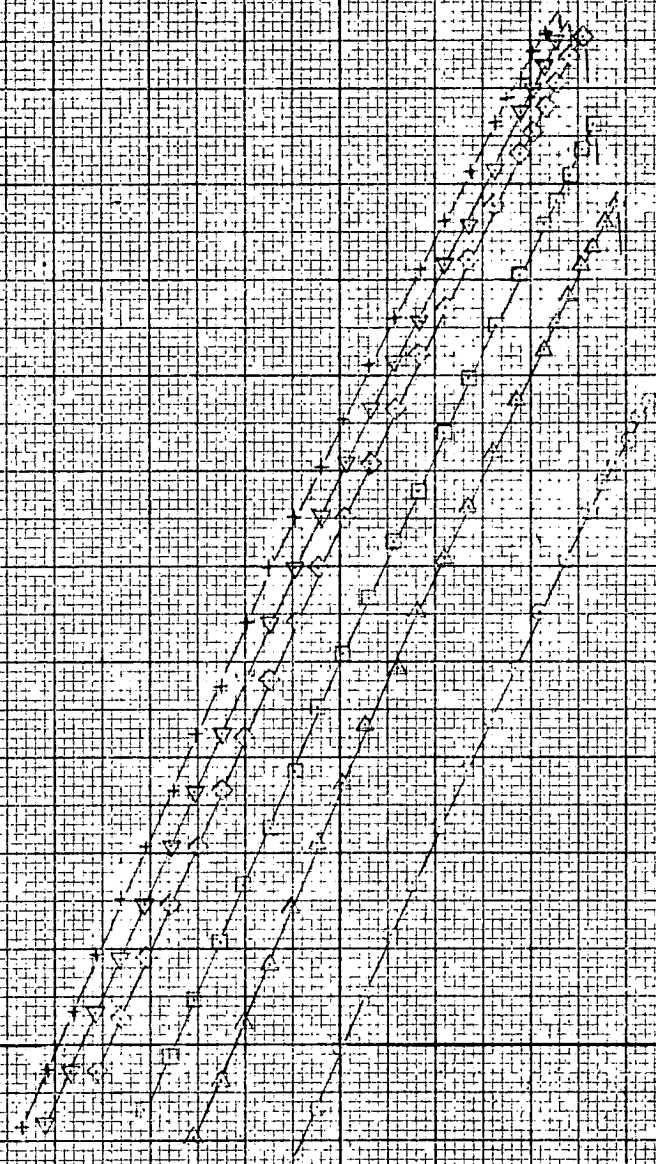


(a) PLAIN FLAP DEFLECTED
 FIGURE 5 - VARIATION OF THE SECTION LIFT COEFFICIENT WITH SECTION ANGLE OF ATTACK FOR THE NACA 63-012 AIRFOIL



SECTION LIFT COEFFICIENT, C_L

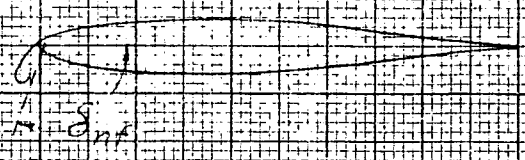
20
16
12
8
4
0
-4
-8
-12
-16



SYMBOL	δ_f
RETRACTED	
▲	10°
▽	20°
△	30°
∇	35°
⊥	40°

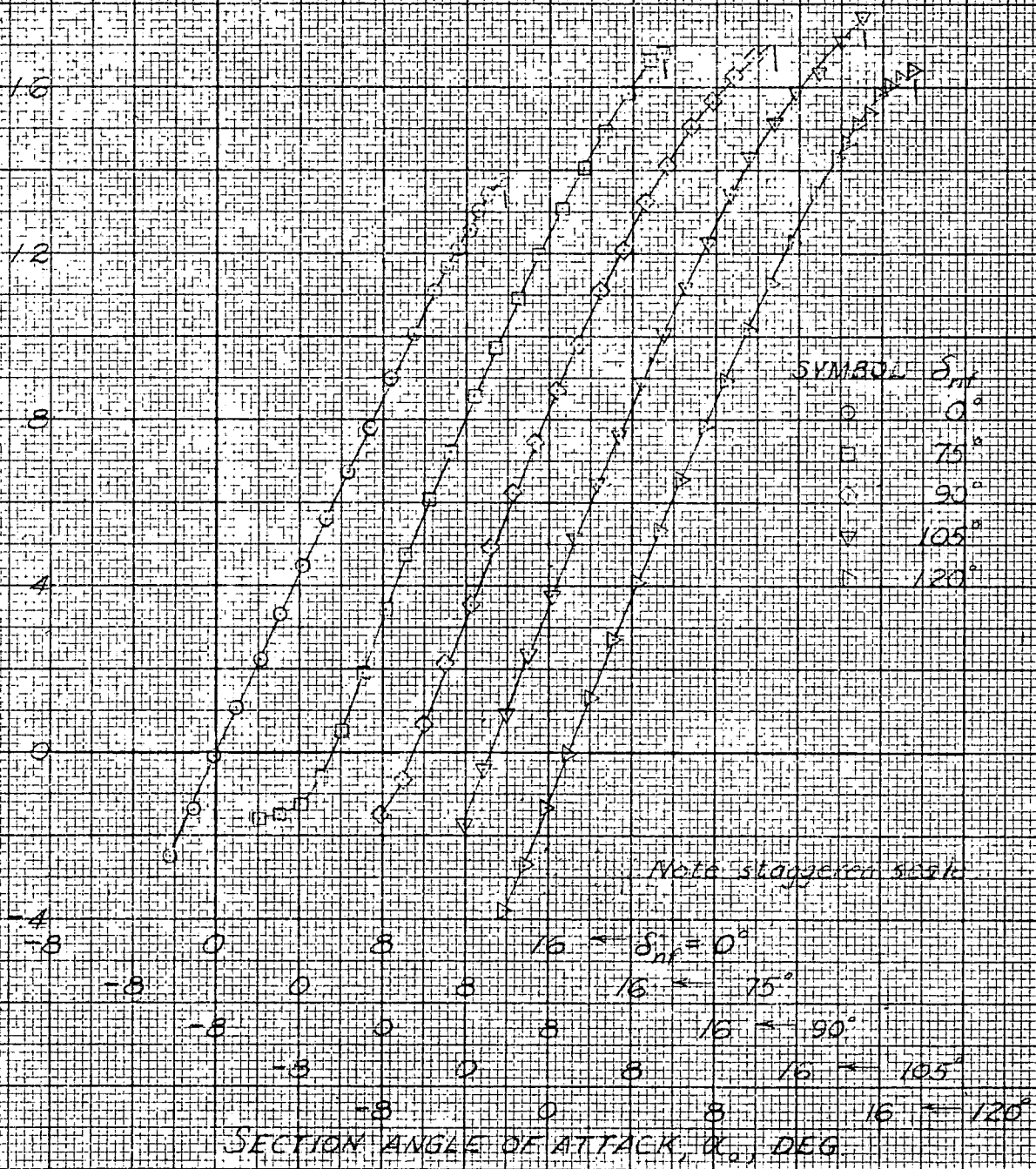
SECTION ANGLE OF ATTACK, α , DEG

FIGURE 5 = CONTINUED. (b) SPLIT FLAP DEFLECTED



SECTION LIFT COEFFICIENT, C_L

SECTION ANGLE OF ATTACK, α , DEG

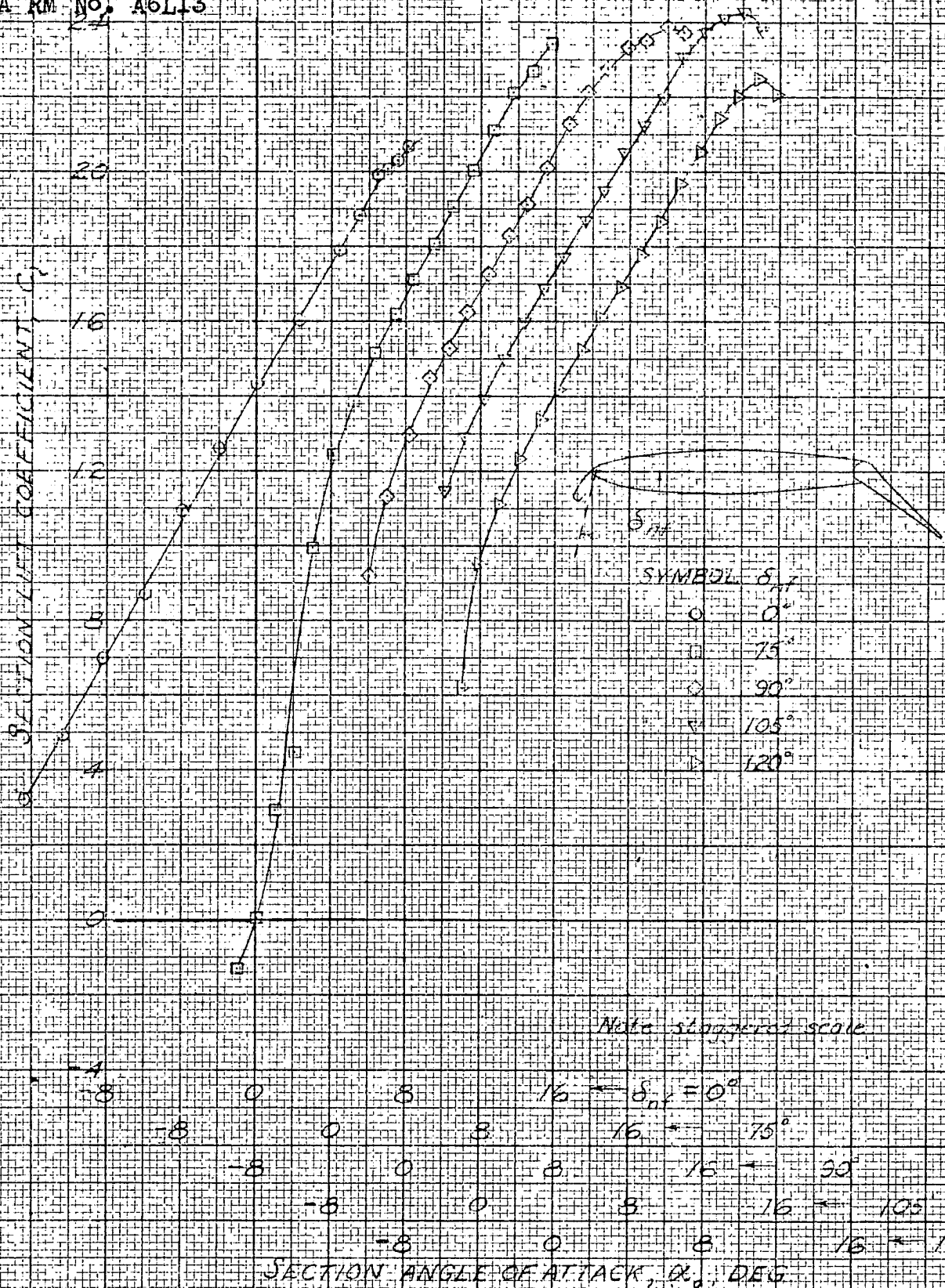


SYMBOL	δ_{nf}
○	0°
□	75°
◇	90°
▽	105°
△	120°

Note staggered scale

(C) NOSE FLAP DEFLECTED

FIGURE 5 - CONTINUED



(1) NOSE FLAP DEFLECTED, PLAIN FLAP DEFLECTED 40°

FIGURE 5 - CONCLUDED

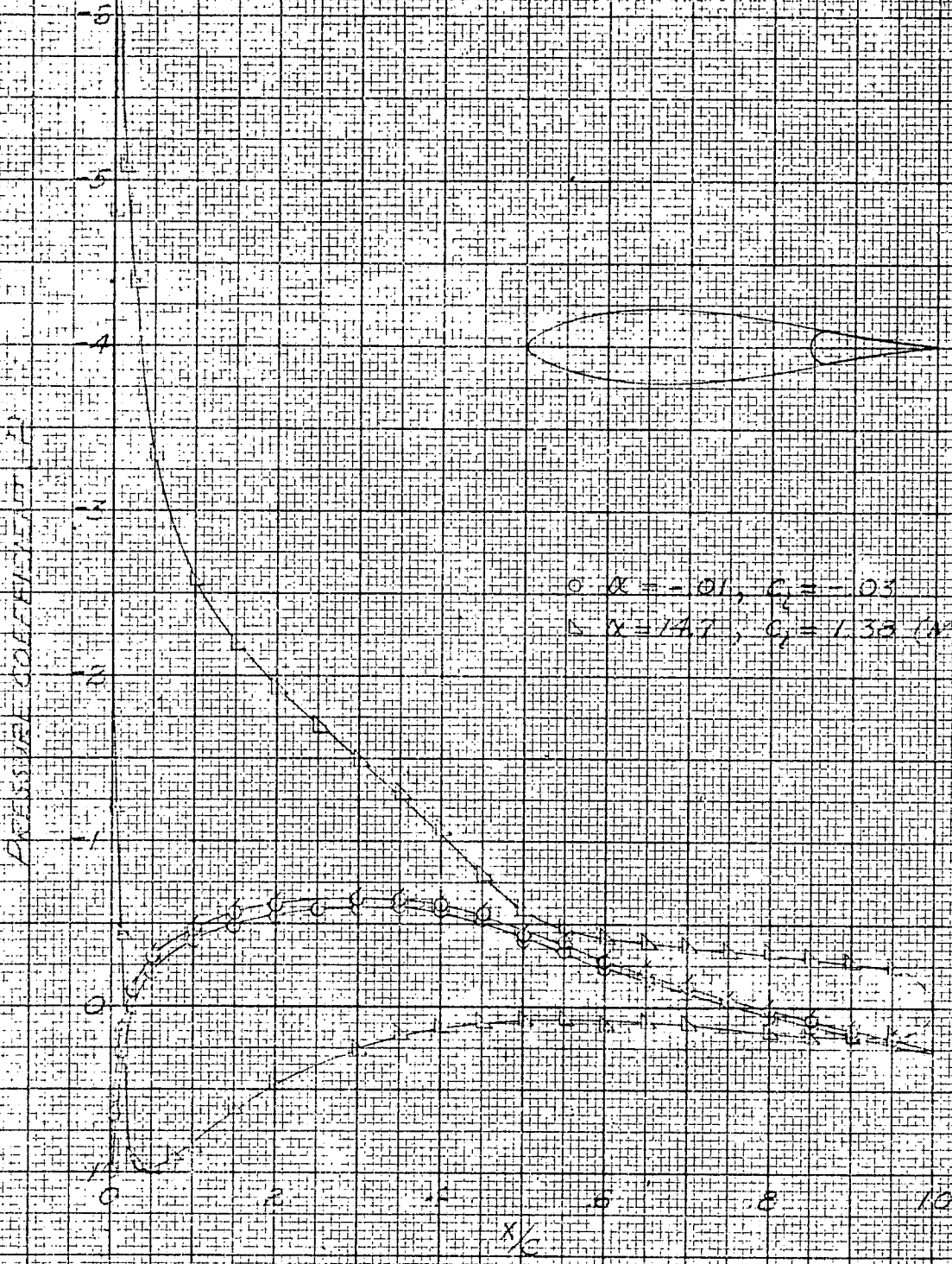
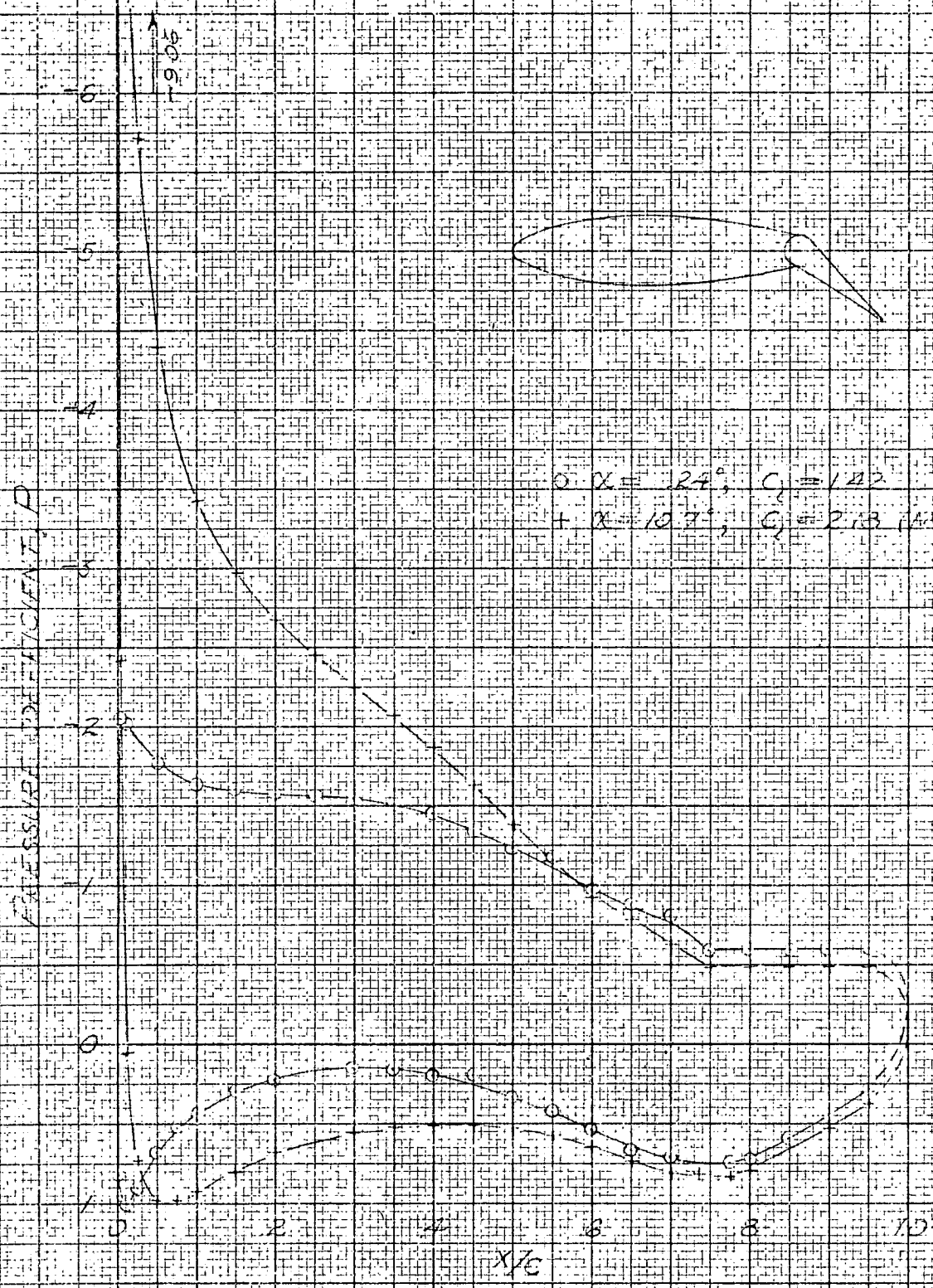


FIGURE 6 - PRESSURE DISTRIBUTION OVER THE NACA 63-018 AIRFOIL



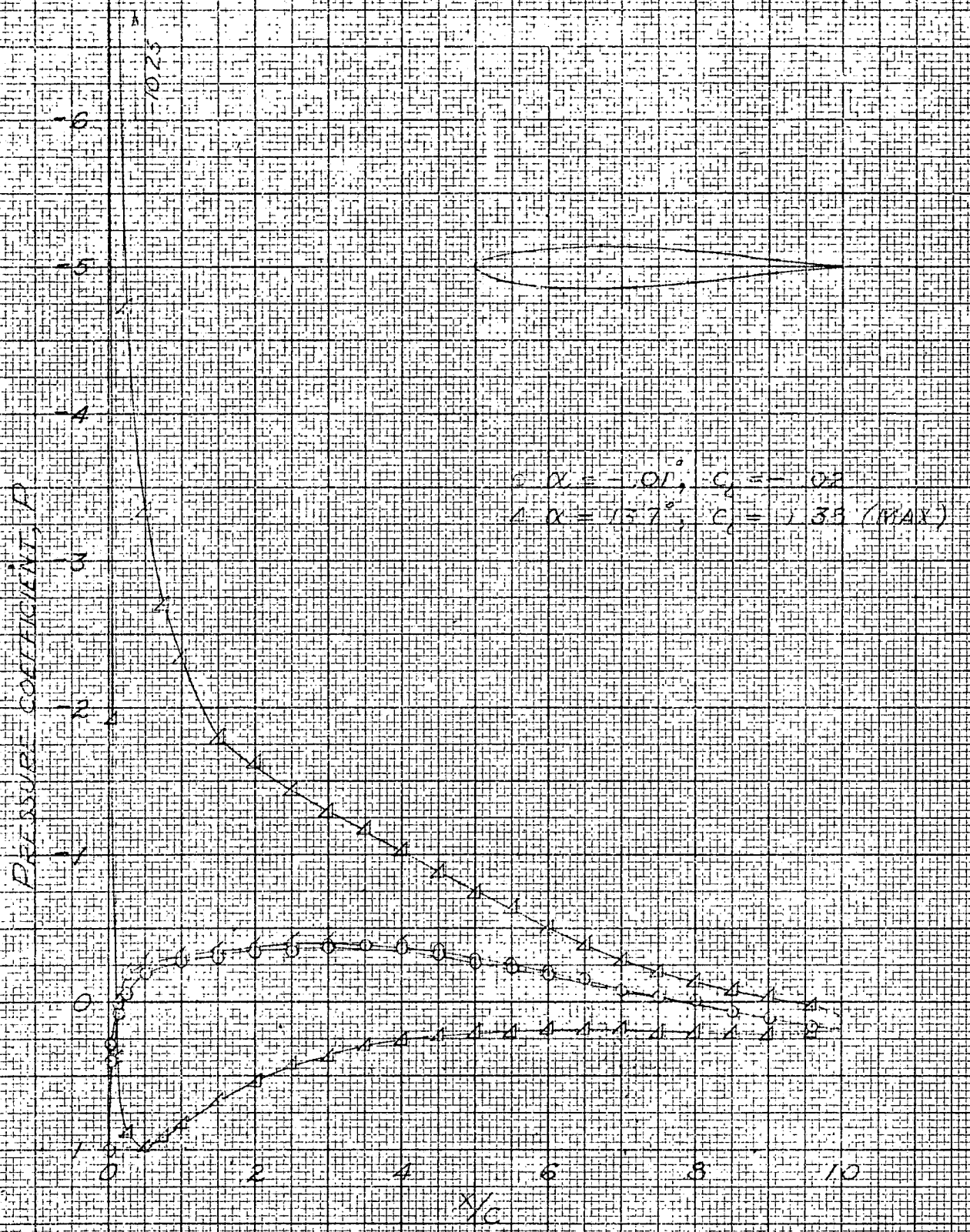
(b) PLAIN FLAP DEFLECTED 40°

FIGURE 6 - CONTINUED.

PRESURE COEFFICIENT, P



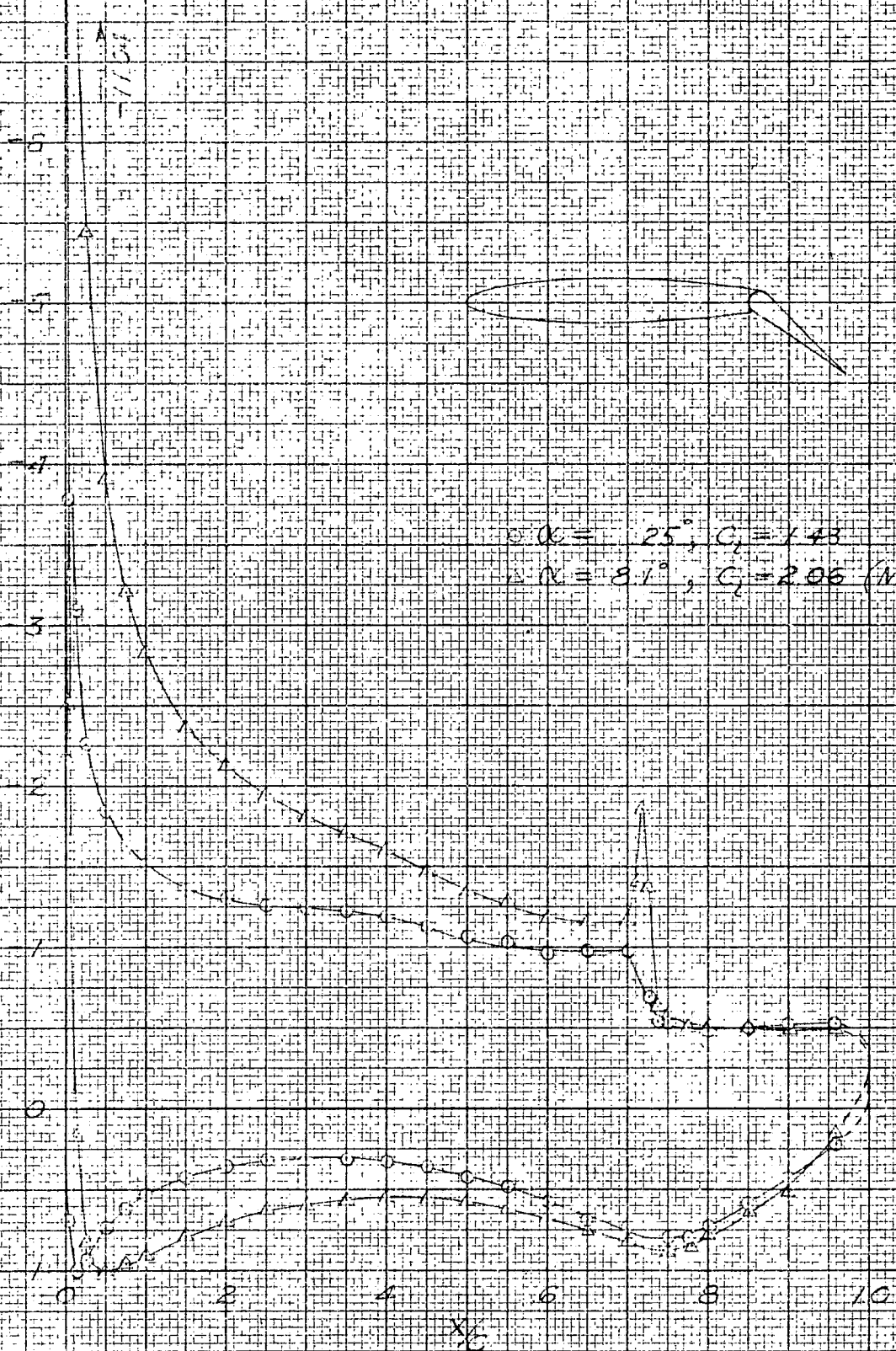
(C) SPLIT FLAP DEFLECTED 40°
 FIGURE 6 - CONCLUDED



$\alpha = -1.01^\circ, C_p = -0.2$
 $\alpha = 13.7^\circ, C_p = 1.35 \text{ (MAX)}$

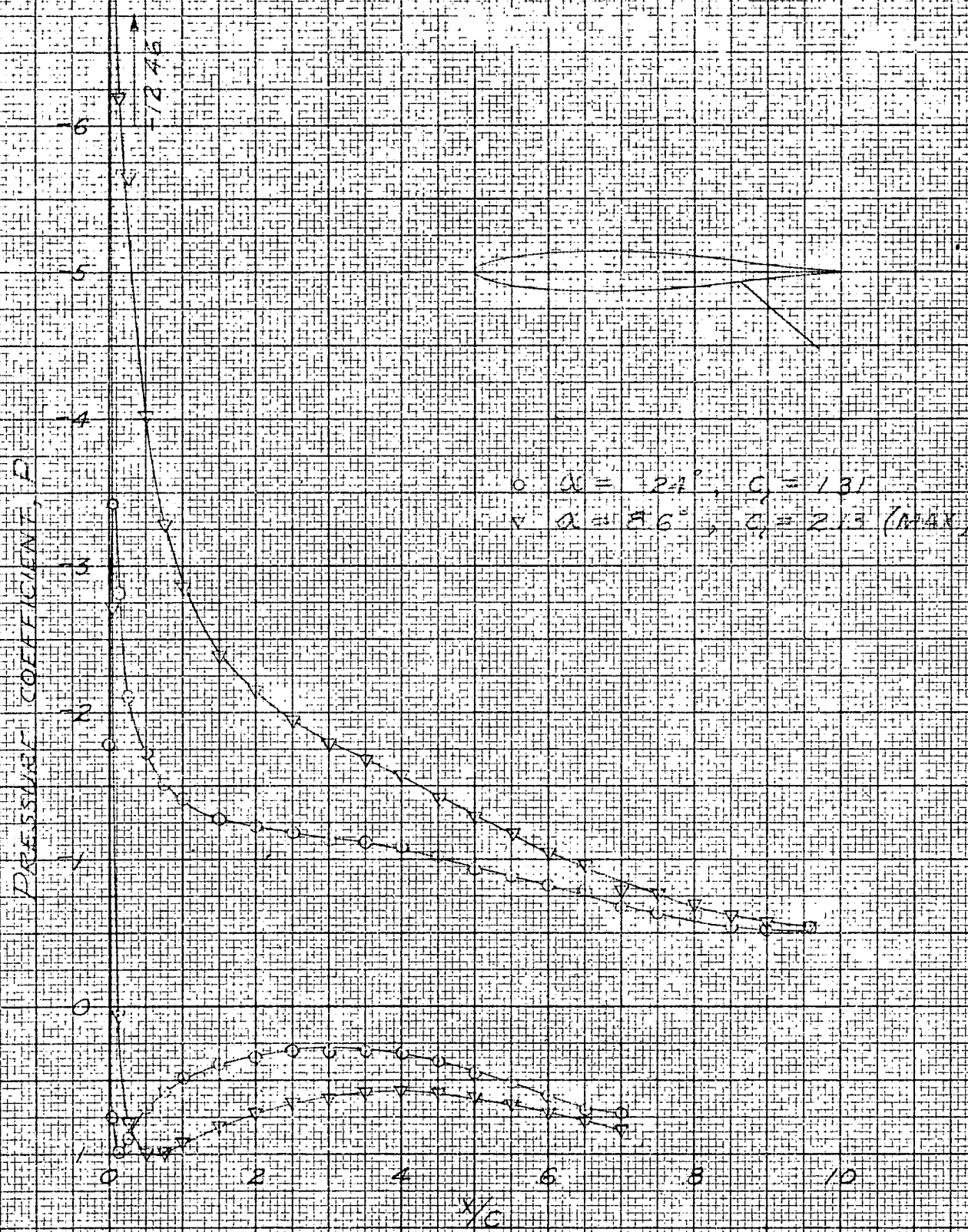
(c) PLAIN FLAP UNDEFLECTED
 FIGURE 7 - PRESSURE DISTRIBUTION OVER THE
 NACA 63-012 AIRFOIL

PRESSURE COEFFICIENT, C_p

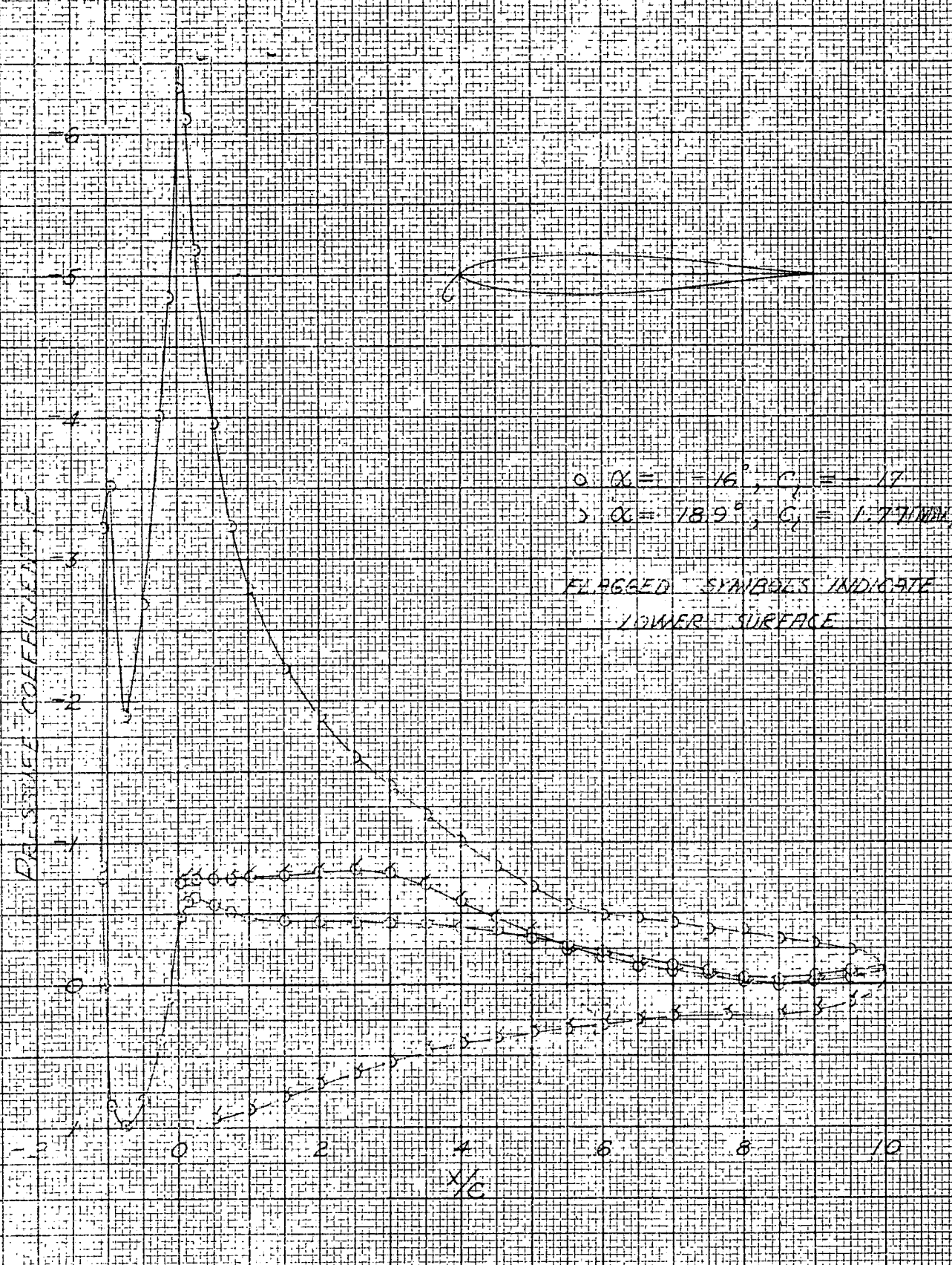


(b) PLAIN FLAP DEFLECTED 40°

FIGURE 7 - CONTINUED.

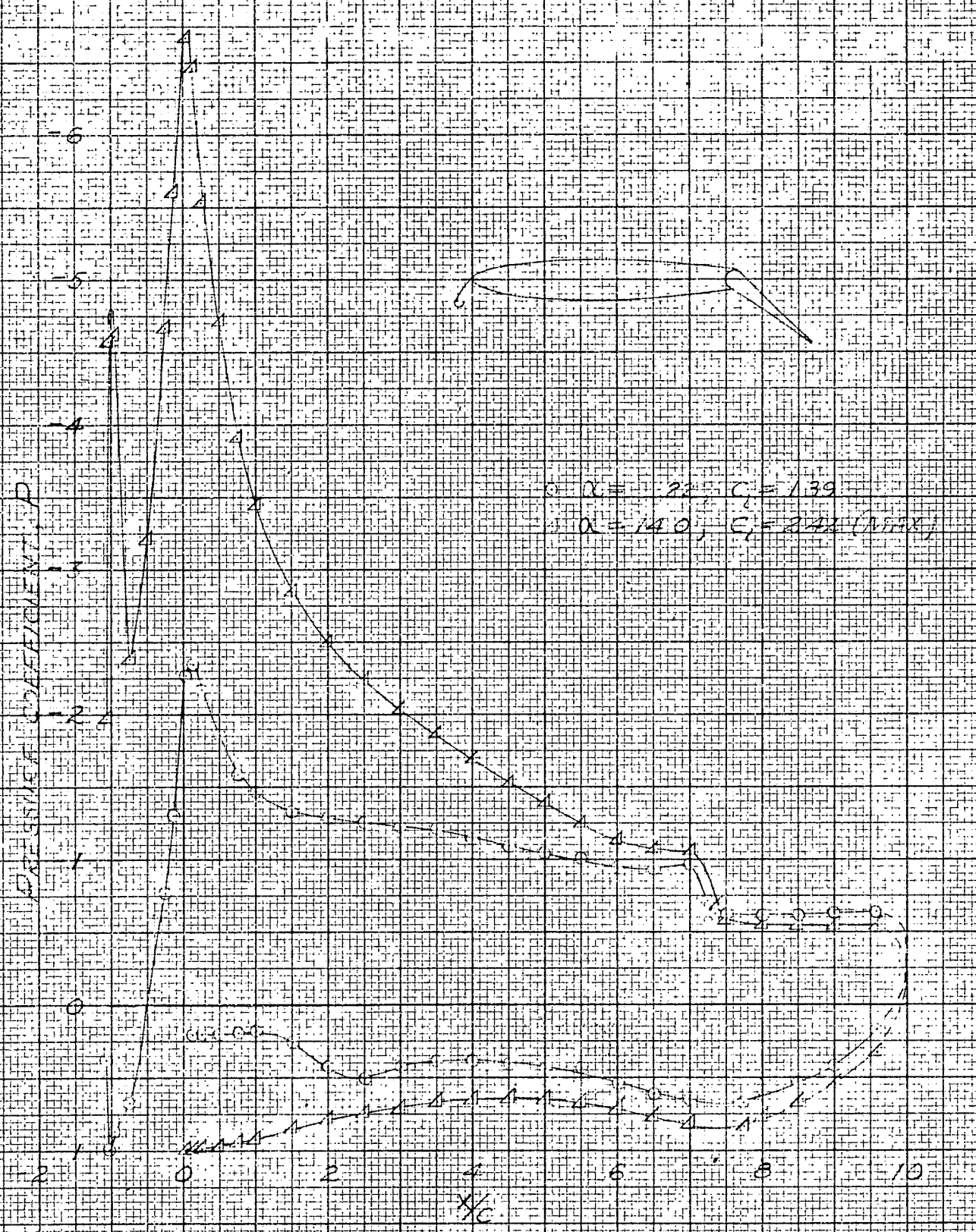


31 SPLIT FLAP DEFLECTED 40°
 FIGURE 7 - CONTINUED

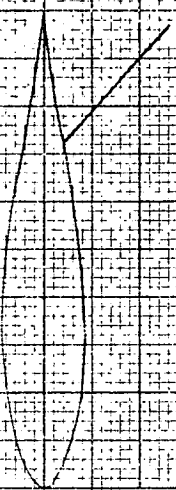


(d) NOSE FLAP DEFLECTED 105°

FIGURE 7 - CONTINUED

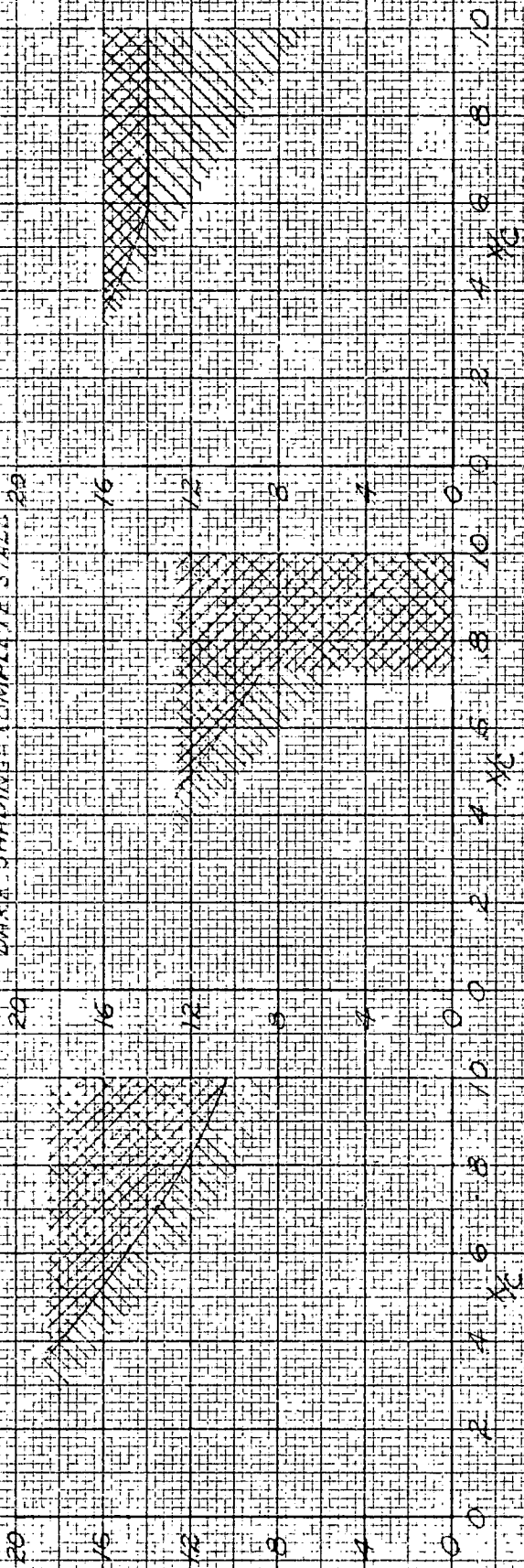


NOSE FLAP DEFLECTED 105°, PLAIN FLAP DEFLECTED 47°
FIGURE 7 - CONCLUDED.



SECTION ANGLE OF ATTACK, α , DEG

LIGHT SHADING = REGION FLOW
 DARK SHADING = COMPLETE STALL

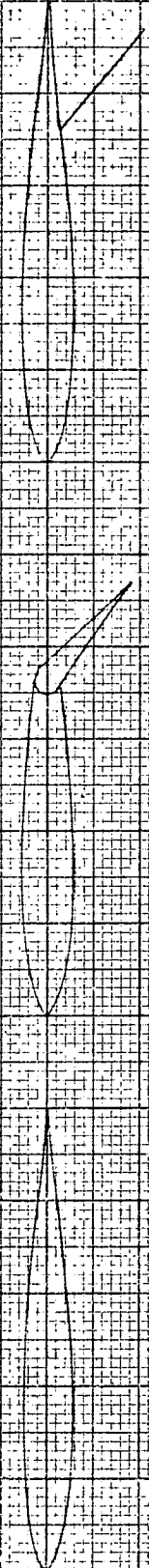


(a) PLAIN AIRFOIL

(b) PLAIN FLAP 40°

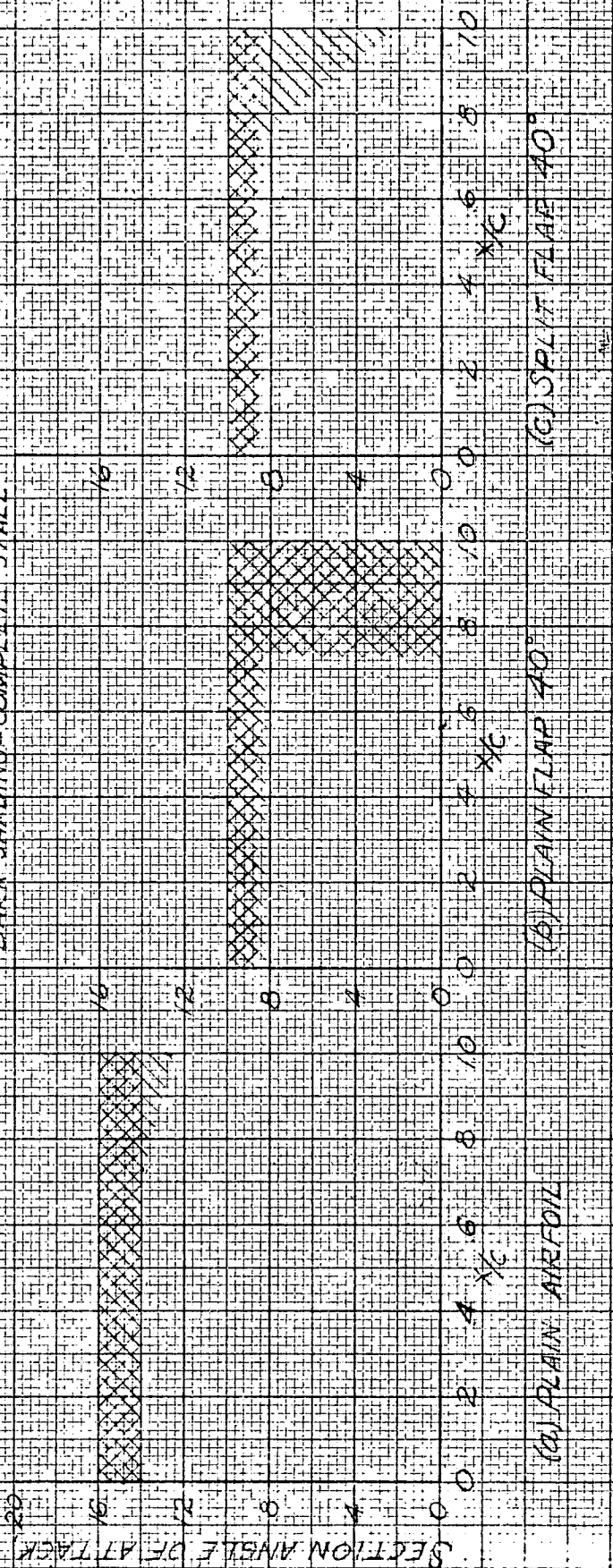
(c) SPLIT FLAP 40°

FIGURE 8. STALLING CHARACTERISTICS OF THE NACA 63-018 AIRFOIL AS INDICATED BY FLUT STUDIES



1. LIGHT SHADING = ROUGH FLOW
 2. DARK SHADING = COMPLETE STALL

SECTION ANGLE OF ATTACK α , DEG



(a) PLAIN AIRFOIL

(b) PLAIN FLAP 40°

(c) SPLIT FLAP 40°

FIGURE 9 - STALLING CHARACTERISTICS OF THE NACA 63-012 AIRFOIL AS INDICATED BY TUFT STUDIES

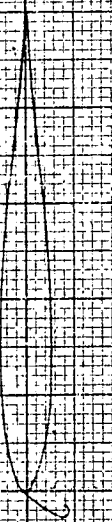


LIGHT SHADING = ROUGH FLOW
 DARK SHADING = COMPLETE STALL

SECTION ANGLE OF ATTACK, α , DEG
 0 1 2 3 4 5 6 7 8 9 10

0 2 4 6 8 10
 $\frac{1}{2}$

(a) NOSE FLAP 105° PLAIN FLAP 40°

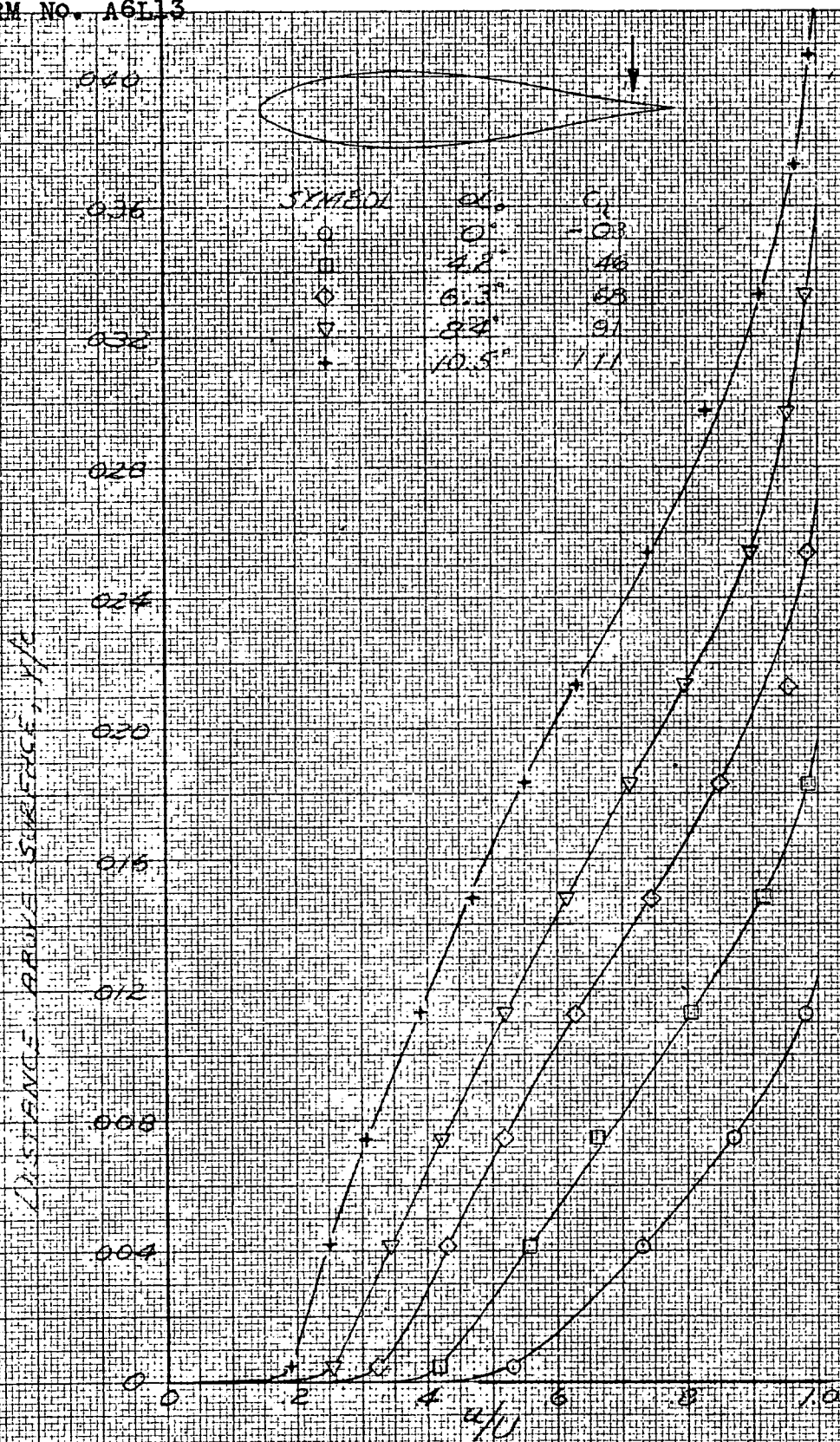


SECTION ANGLE OF ATTACK, α , DEG
 0 1 2 3 4 5 6 7 8 9 10

0 2 4 6 8 10
 $\frac{1}{2}$

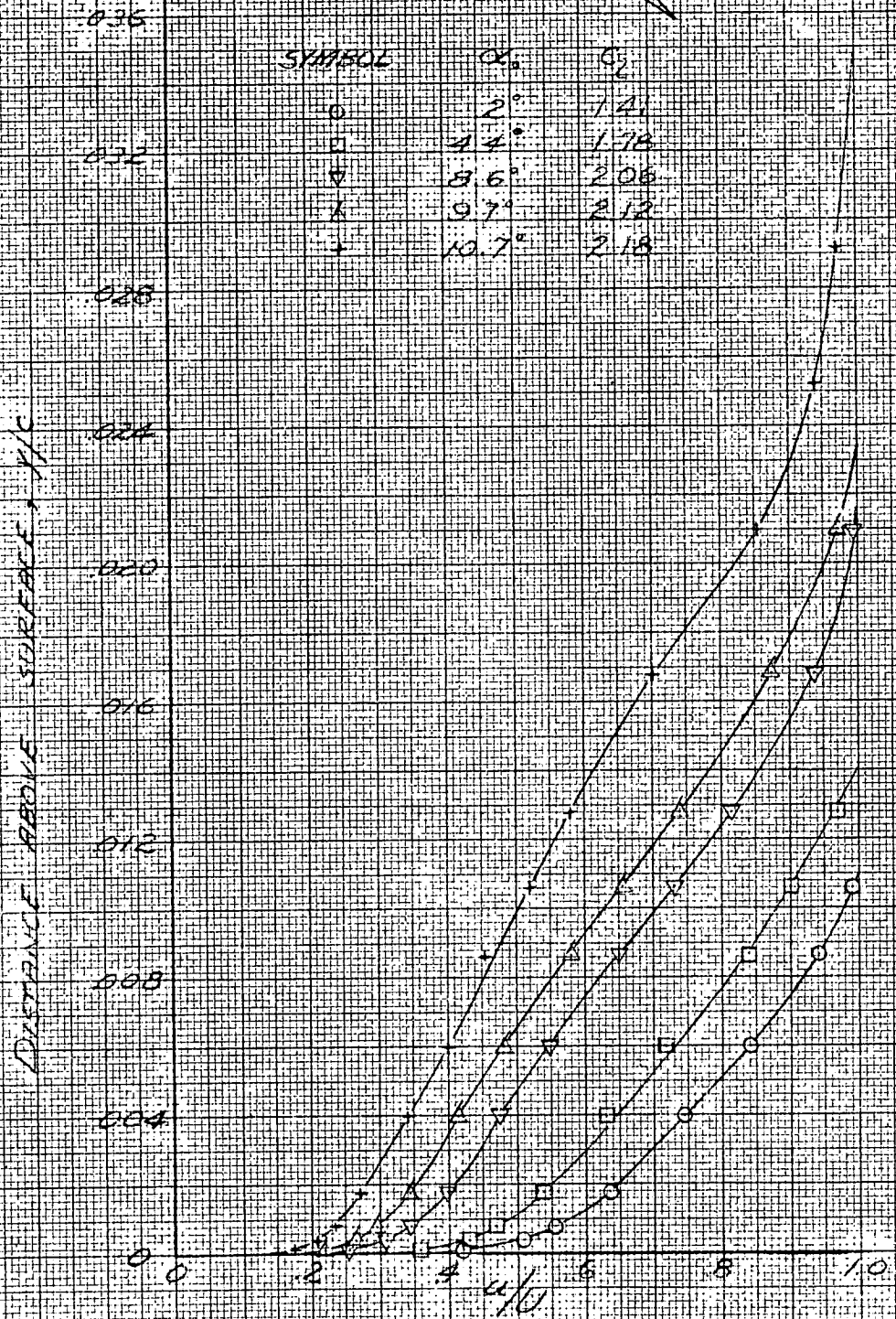
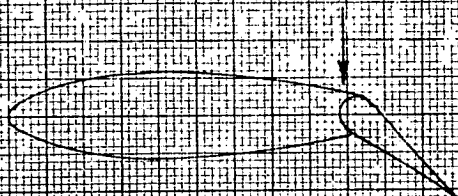
(b) NOSE FLAP 70.5° PLAIN FLAP 0°

FIGURE 9 - CONCLUDED



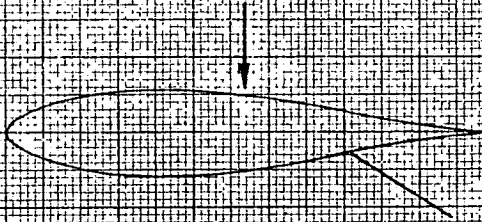
(a) PLAIN FLAP, $\delta_f = 6^\circ$, 90-PERCENT CHORD.

FIGURE 10 - BOUNDARY-LAYER VELOCITY PROFILES FOR THE NACA 63-018 AIRFOIL.



(b) PLAIN FLAP, $\delta_f = 40^\circ$, 70-PERCENT CHORD

FIGURE 10 - CONTINUED.



DISTANCE ABOVE SURFACE, Y/C

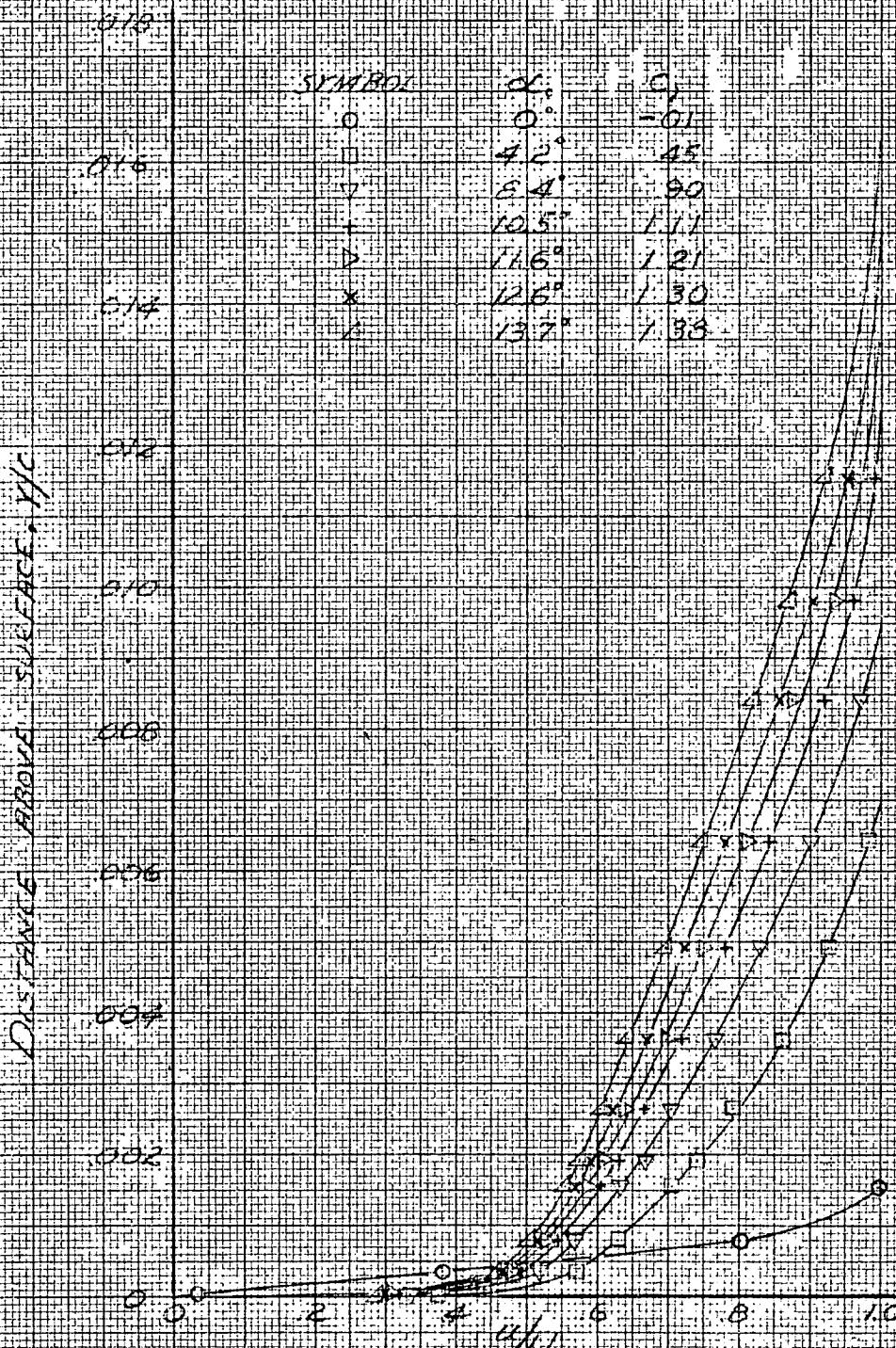
018
016
014
012
010
008
006
004
002
0

SYMBOL	α	C_L
o	3°	1.41
D	4.5°	1.84
v	6.7°	2.25
+	10.8°	2.75
x	12.9°	2.63
Δ	13.0°	2.69

4/11

(C) SPLIT FLAP, $\delta_f = 40^\circ$, 50 PERCENT CHORD.

FIGURE 10 - CONCLUDED



(a) PLAIN FLAP, $\delta_f = 0^\circ$, 45-PERCENT CHORD.

FIGURE 11 - BOUNDARY-LAYER VELOCITY PROFILES FOR THE NACA 63-012 AIRFOIL.



(b) PLAIN FLAP, $\delta = 45^\circ$, 45 PERCENT CHORD.

FIGURE 11 - CONTINUED.

DISTANCE ABOVE SURFACE, h/c

0.40
0.35
0.32
0.28
0.24
0.20
0.15
0.12
0.08
0.04
0.0



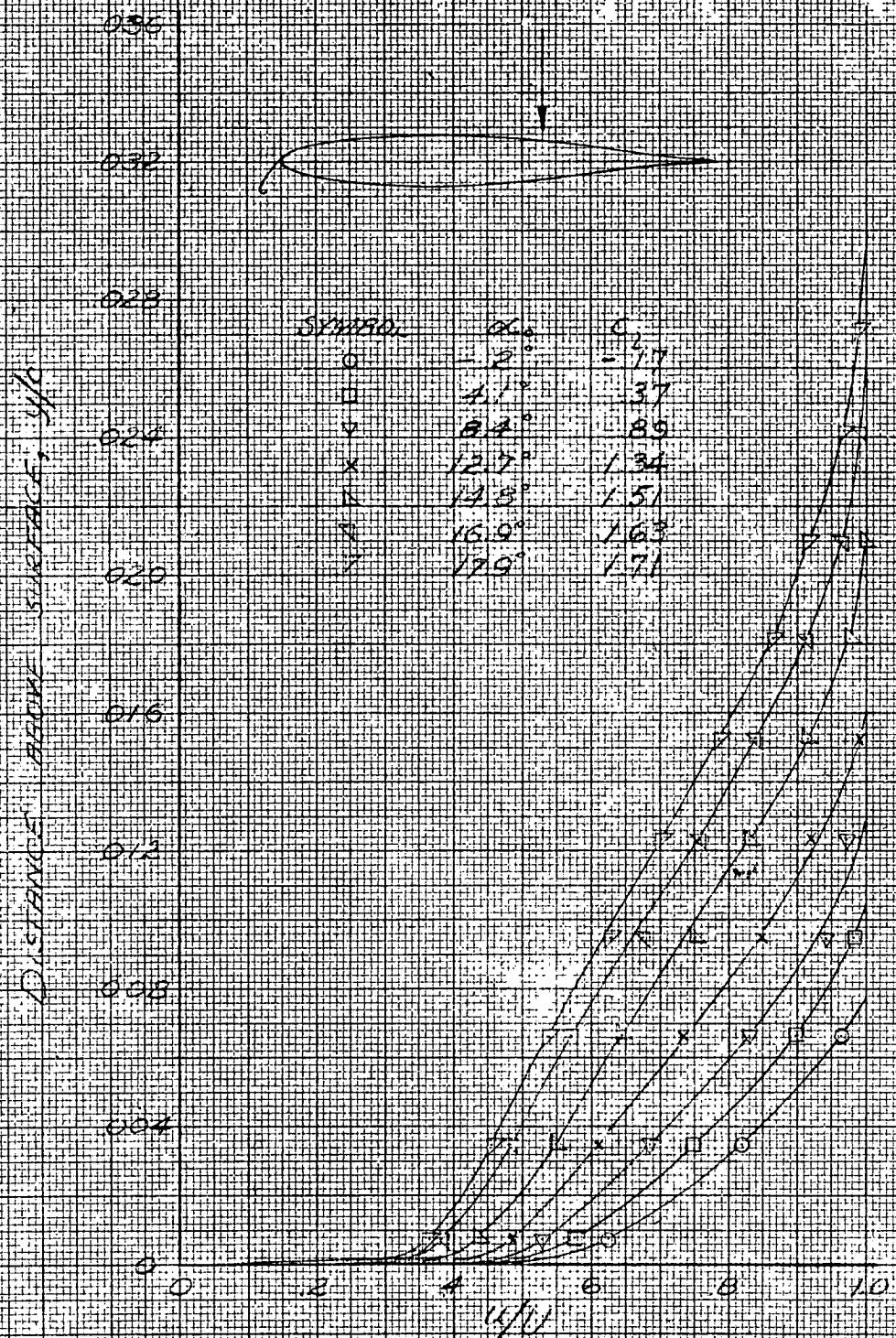
SYMBOL	δ_f	C_L
○	2°	1.31
□	4.4°	1.72
○	6.5°	1.93
○	7.6°	2.02
▽	8.6°	2.13

U/∞

0 0 2 4 6 8 10

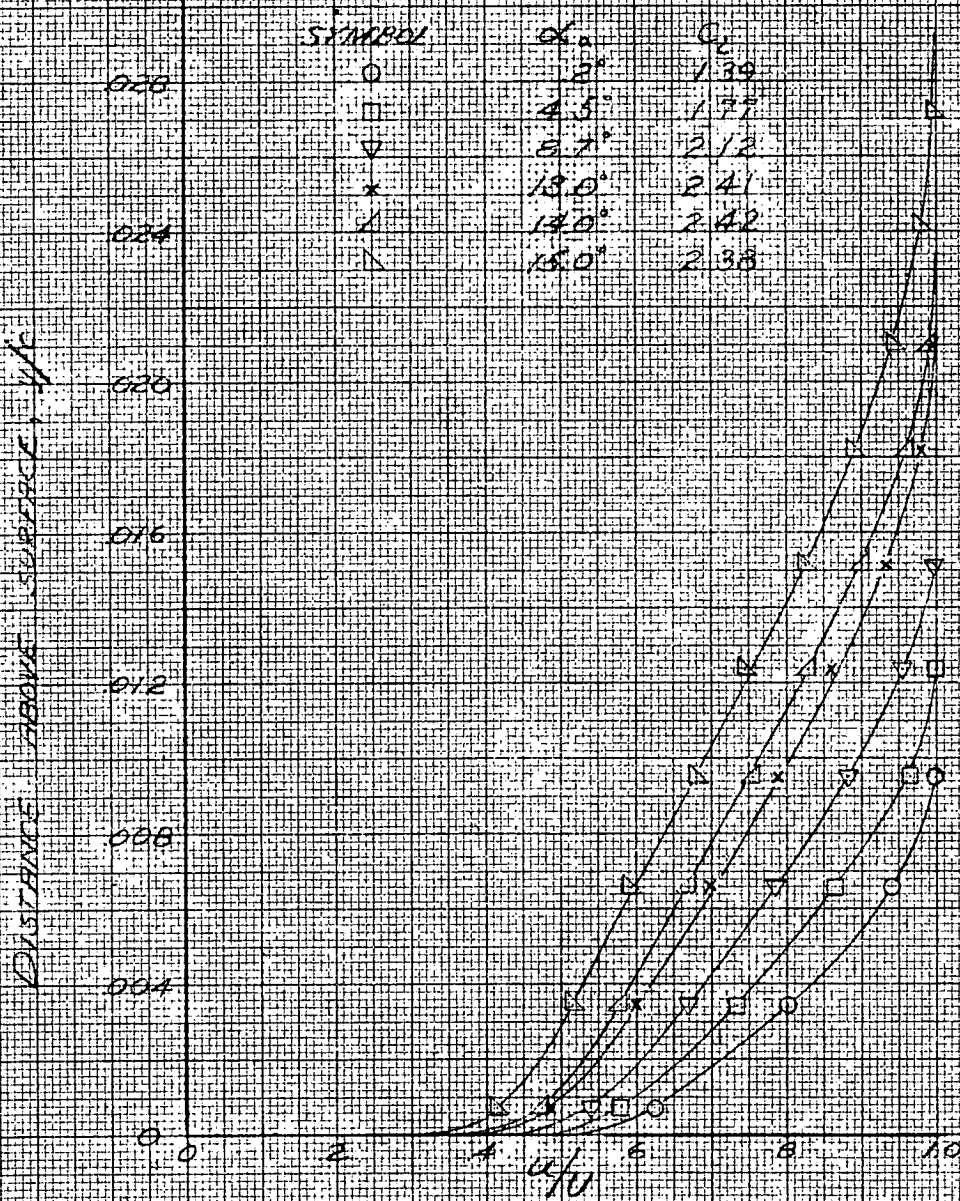
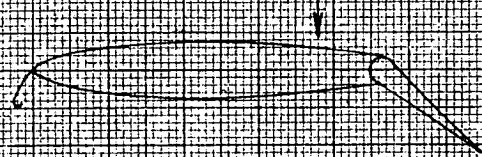
(C) SPLIT FLAP $\delta_f = 40^\circ$, 90 PERCENT CHORD.

FIGURE 11 - CONTINUED.



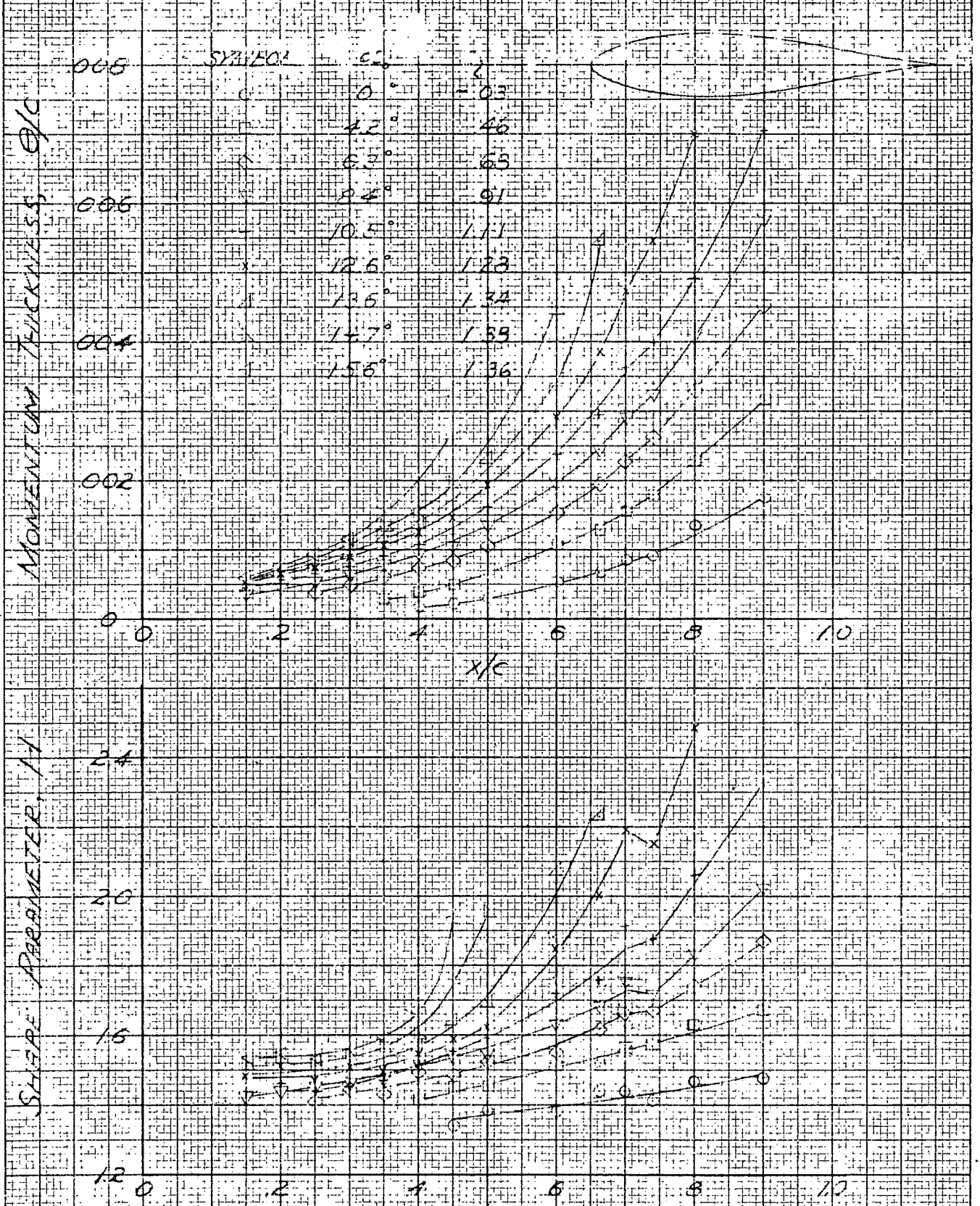
(d) NOSE FLAP, $\delta_n = 10.5^\circ$
 PLAIN FLAP, $\delta_f = 0^\circ$, 50-PERCENT CHORD.

FIGURE 11 - CONTINUED.



(C) NOSE FLAP, $\delta_{nose} = 105^\circ$
 PLAIN FLAP $\delta_f = 90^\circ$, 60-PERCENT CHORD.

FIGURE 11 - CONCLUDED.



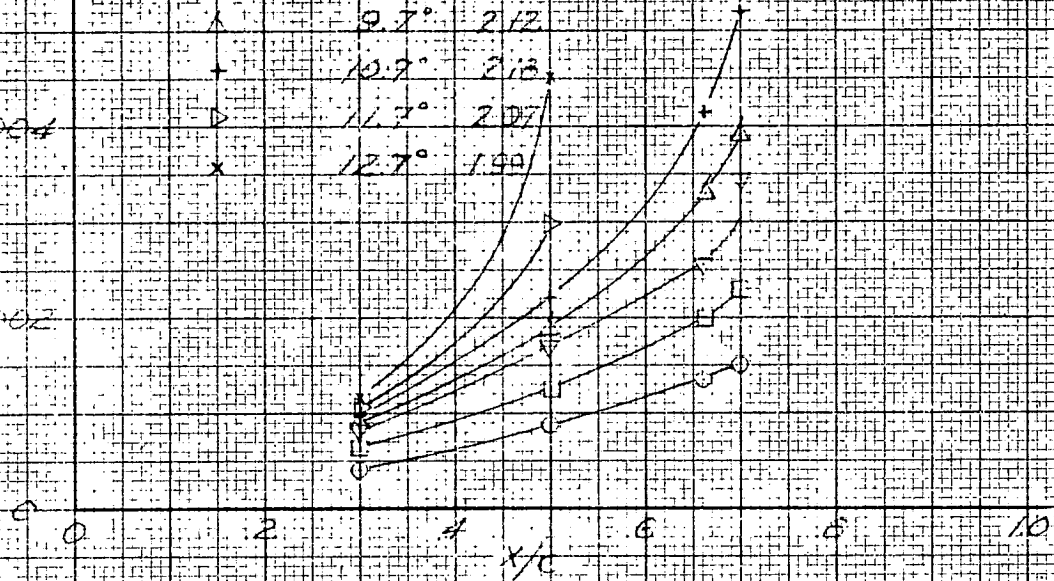
(1) PLAIN FLAP, $\delta_f = 0^\circ$.

FIGURE 12 - VARIATION OF THE BOUNDARY-LAYER MOMENTUM THICKNESS AND SHAPE PARAMETER ALONG THE SURFACE OF THE NACA 53 AIRFOIL



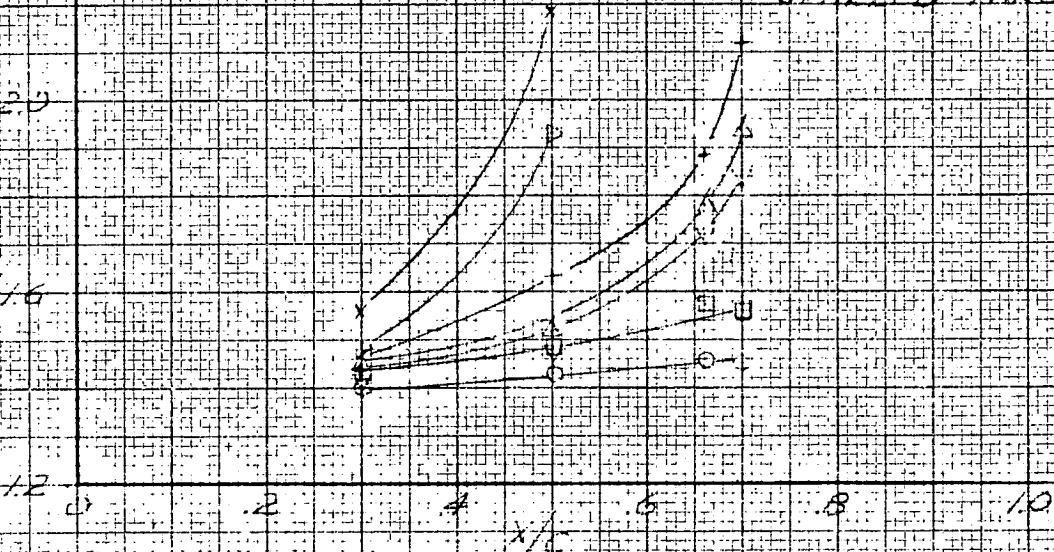
MOMENTUM THICKNESS, θ/c

SYMBOL	α	C_L
○	2°	1.41
□	4.4°	1.75
▽	8.6°	2.06
▲	9.7°	2.12
+	10.9°	2.18
△	11.7°	2.07
x	12.7°	



SHAPE PARAMETER, H

NOTE: - FLAP (LAST 0.275c) COMPLETELY STALLED THROUGHOUT



(b) FLAIN FLAP, $\delta_f = 40^\circ$
 FIGURE 12 - CONTINUED.



MOMENTUM THICKNESS, θ/c

0.02
0.04
0.06
0.08

SYMBOL	α_0	C_D
○	3°	1.51
□	4.5°	1.64
▽	8.7°	2.25
+	10.8°	2.45
x	12.5°	2.63
△	13.9°	2.65

x/c

0 2 4 6 8 10

SLIP STREAM PARAMETER, H

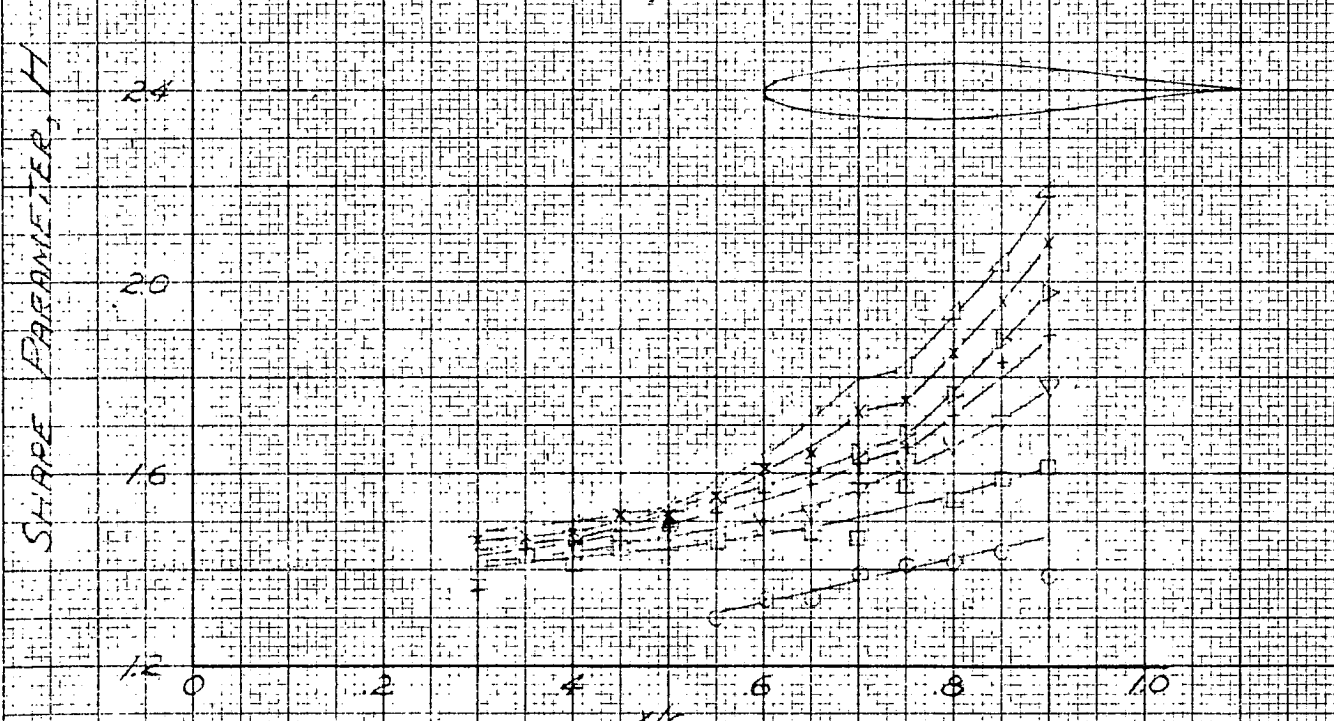
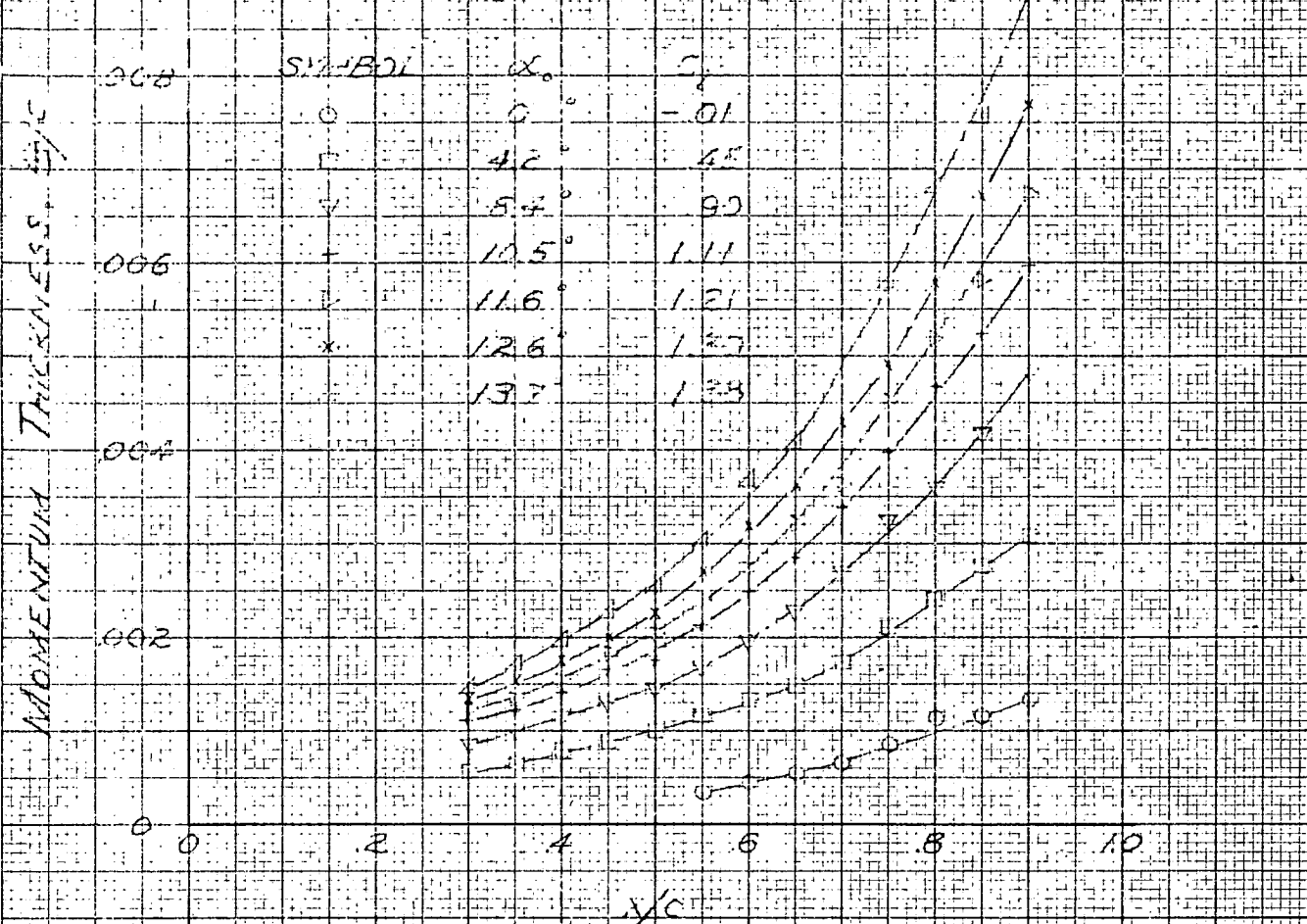
1.5
2.0
2.4

x/c

0 2 4 6 8 10

(C) SPILT FLAP $\delta_f = 40^\circ$

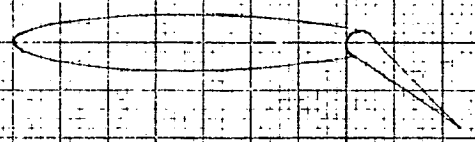
FIGURE 12 - CONCLUDED



(a) FLUID FLAT, $\delta_0 = 0^\circ$

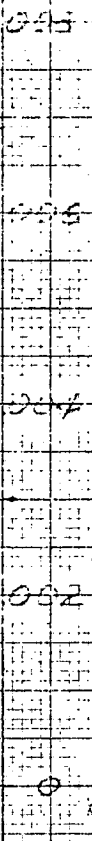
FIGURE 13 - VARIATION OF THE BOUNDARY-LAYER MOMENTUM THICKNESS AND SHAPE PARAMETER

- FLOWING THE SURFACE OF THE NACA 17.63-012 AIRFOIL

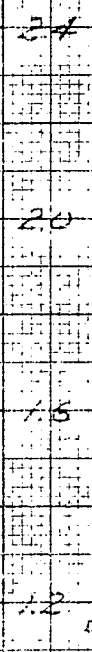


SYMBOL	α_0	C_L
○	3°	1.43
□	4.5°	1.73
◇	6.5°	1.53
⊙	7.6°	2.02

MOMENTUM THICKNESS, θ/c



SHAPE PARAMETER, H



NOTE: - FLAP (LAST 33.75%) COMPLETELY STALLED THROUGHOUT

(b) PLAIN FLAP, $\delta_f = 40^\circ$

FIGURE 13 - CONTINUED

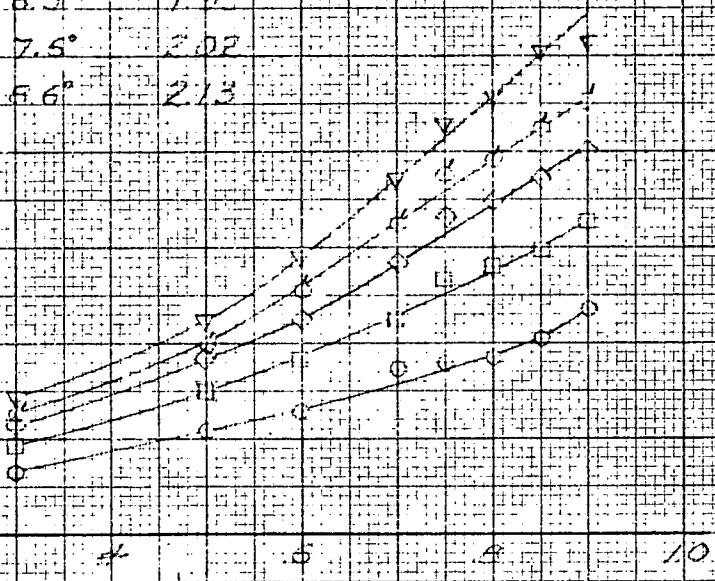
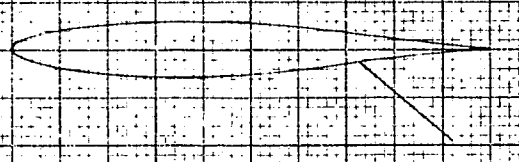
THICKNESS, %

MOMENTUM

SHAPE PARAMETERS, H

005
006
007
008
009
010
011
012
013
014
015
016
017
018
019
020
021
022
023
024
025
026
027
028
029
030
031
032
033
034
035
036
037
038
039
040
041
042
043
044
045
046
047
048
049
050
051
052
053
054
055
056
057
058
059
060
061
062
063
064
065
066
067
068
069
070
071
072
073
074
075
076
077
078
079
080
081
082
083
084
085
086
087
088
089
090
091
092
093
094
095
096
097
098
099
100

SYMBOL	α	C
○	2°	1.81
□	4.4°	1.72
◇	6.5°	1.93
⊗	7.5°	2.02
▽	8.6°	2.13



(C) SPLIT FLAP, $\alpha = 40^\circ$

FIGURE 13 - CONTINUED.

MOMENTUM THICKNESS, θ/c

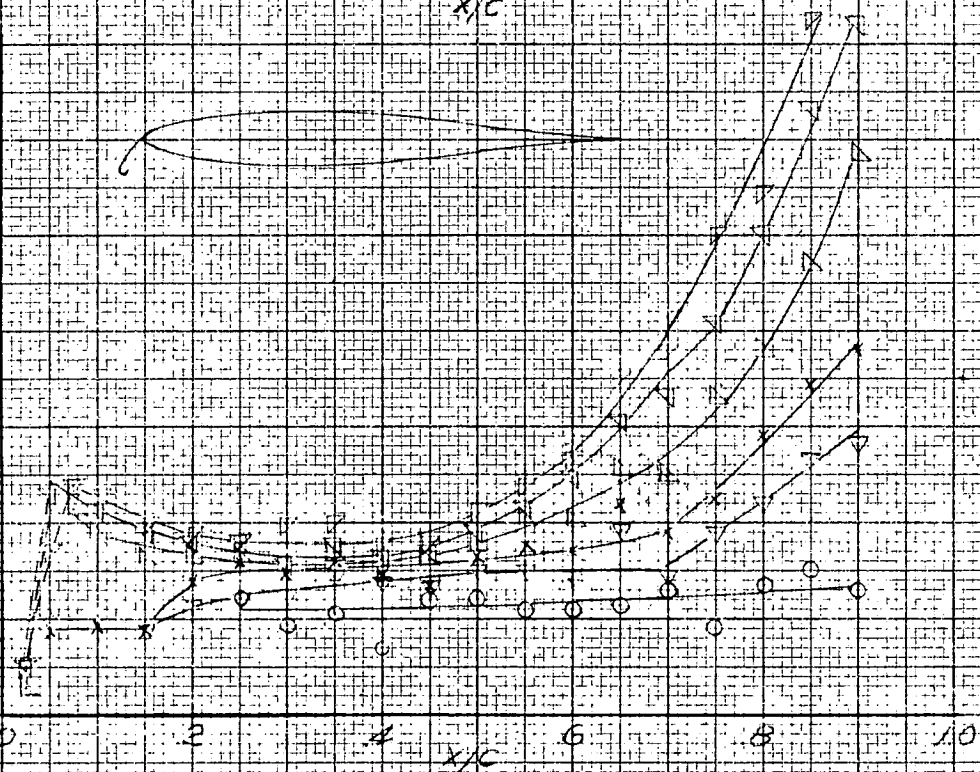
0.08
0.06
0.04
0.02

SYMBOL	α°	C_L
o	-2	.17
.	4	.31
v	8.4	.49
x	12.7	.74
s	14.8	.91
7	15.0	1.03
7	17.9	1.71

x/c

SHAPE PARAMETER, H

2.4
2.0
1.6
1.2



(a) PLAIN FLAP, $\delta_f = 0^\circ$
 NOSE FLAP, $\delta_{nf} = 105^\circ$

FIGURE 13 - CONTINUED.

605

S/C

605

605

605

24

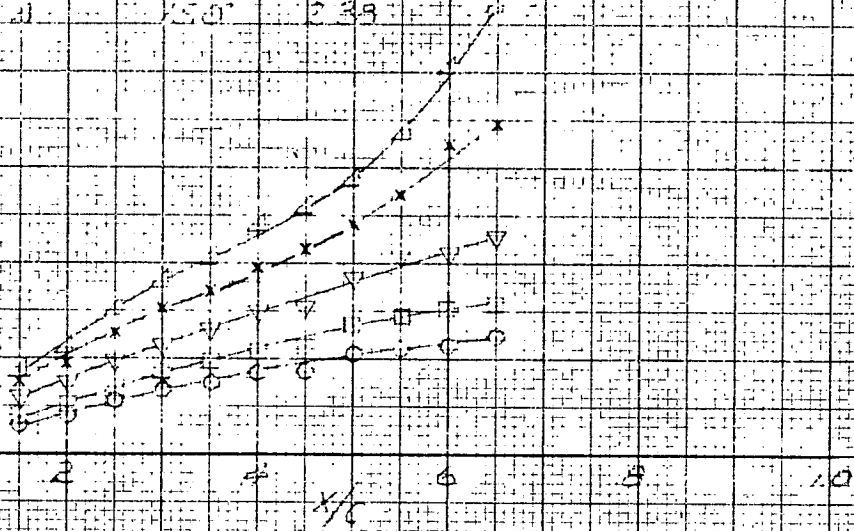
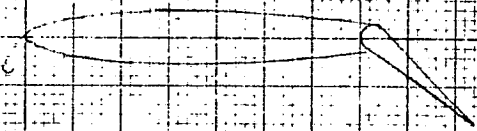
20

16

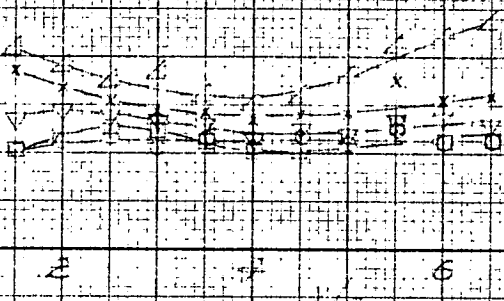
12

CIRCUIT PERCENTAGE, %

ANGLE	α_0	C_L
0	2°	1.39
1	15°	1.77
2	37°	2.18
3	50°	2.41
4	50°	2.39



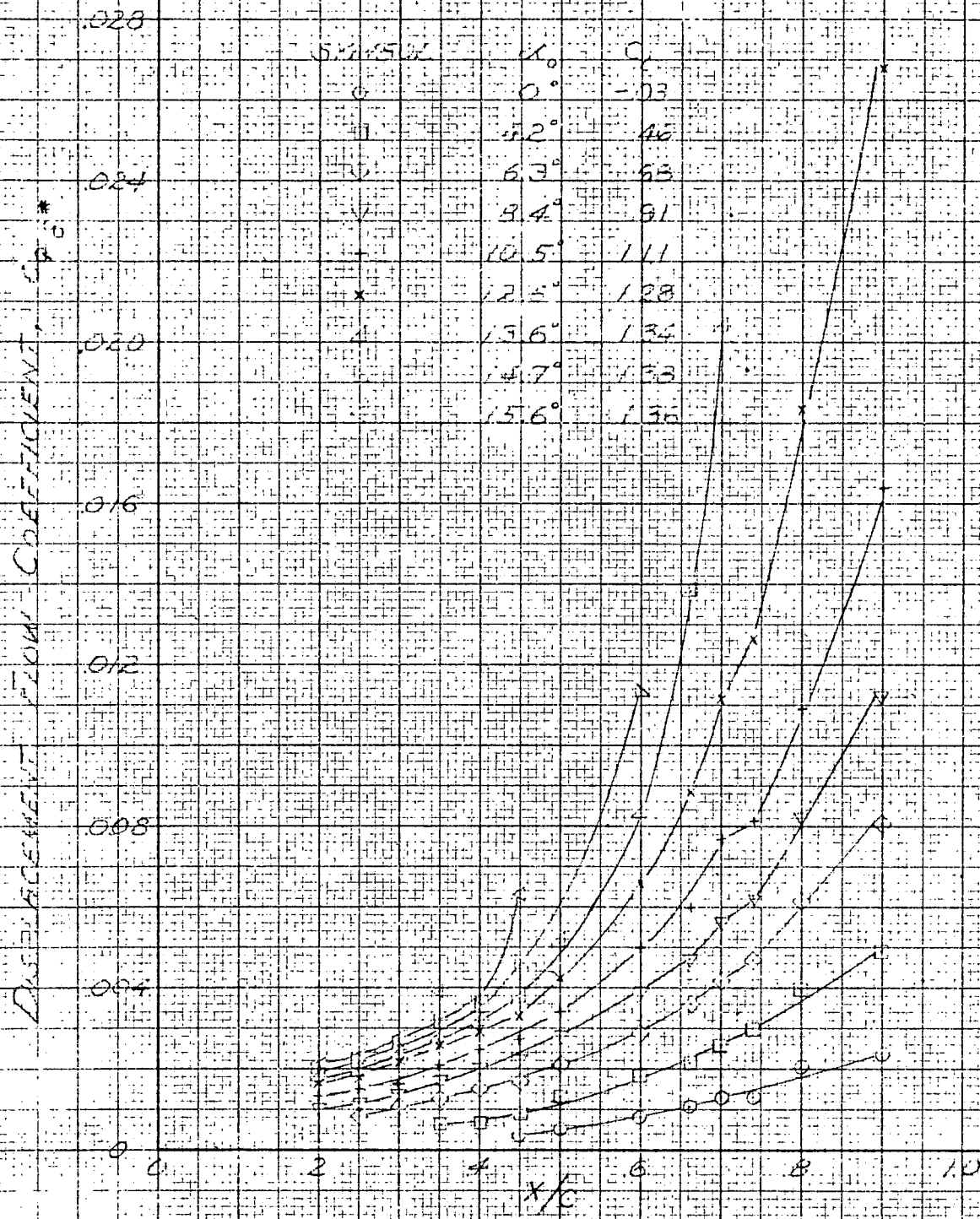
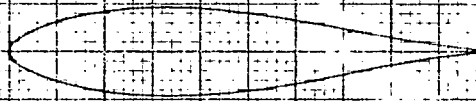
NOTE: - FLAP (LAST 0.275 C) COMPLETELY STALLED THROUGHOUT



(a) PLAIN FLAP $\delta = 40^\circ$

NOTE FLAP $\delta = 105^\circ$

FIGURE 13 - CONE WIND



(a) FLAT FLAP UNDEFLECTED.

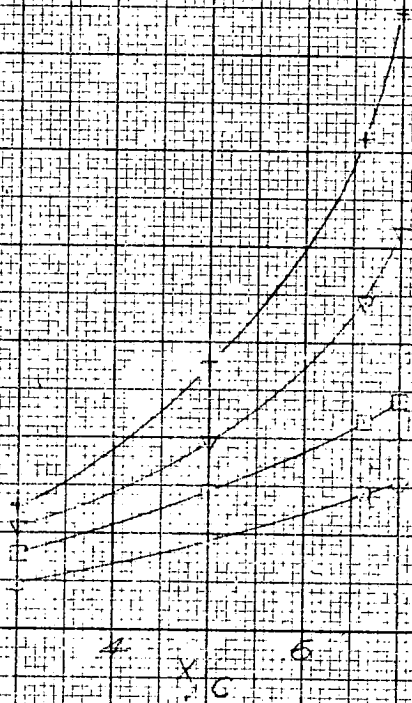
FIGURE 17 - VARIATION OF THE DISPLACEMENT FLOW COEFFICIENT ALONG THE SURFACE OF THE WACA 63-015 AIRFOIL



DISPLACEMENT FLOW COEFFICIENT, C_{df}

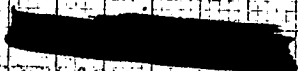
0.04
0.03
0.02
0.01
0

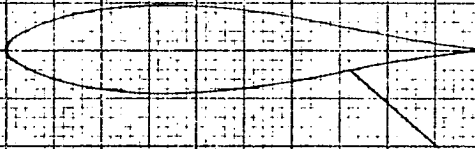
SYMBOL	α	C_{df}
○	2°	1.41
□	4.4°	1.78
▽	8.8°	2.56
×	10.7°	2.78



(b) PLAIN FLAP DEFLECTED 40°

FIGURE 14 - CONTINUED

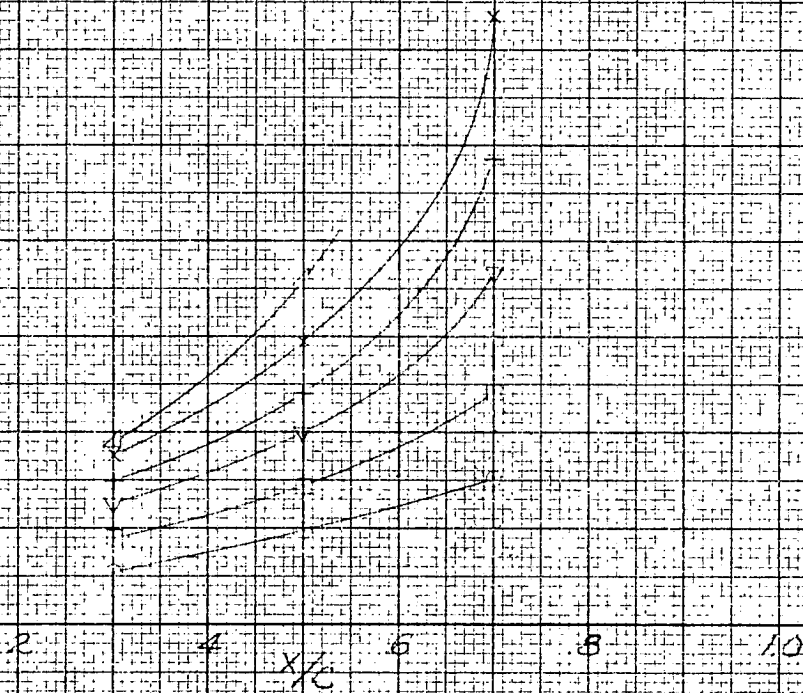




DISPLACEMENT FLOW COEFFICIENT C_{DF}

0.25
0.24
0.22
0.18
0.12
0.08
0.04
0

SYMBOL	α_n	C_{DF}
o	3	1.41
D	4.5	1.84
v	6.7	2.25
+	10.8	2.45
x	12.9	2.63
4	13.9	2.69



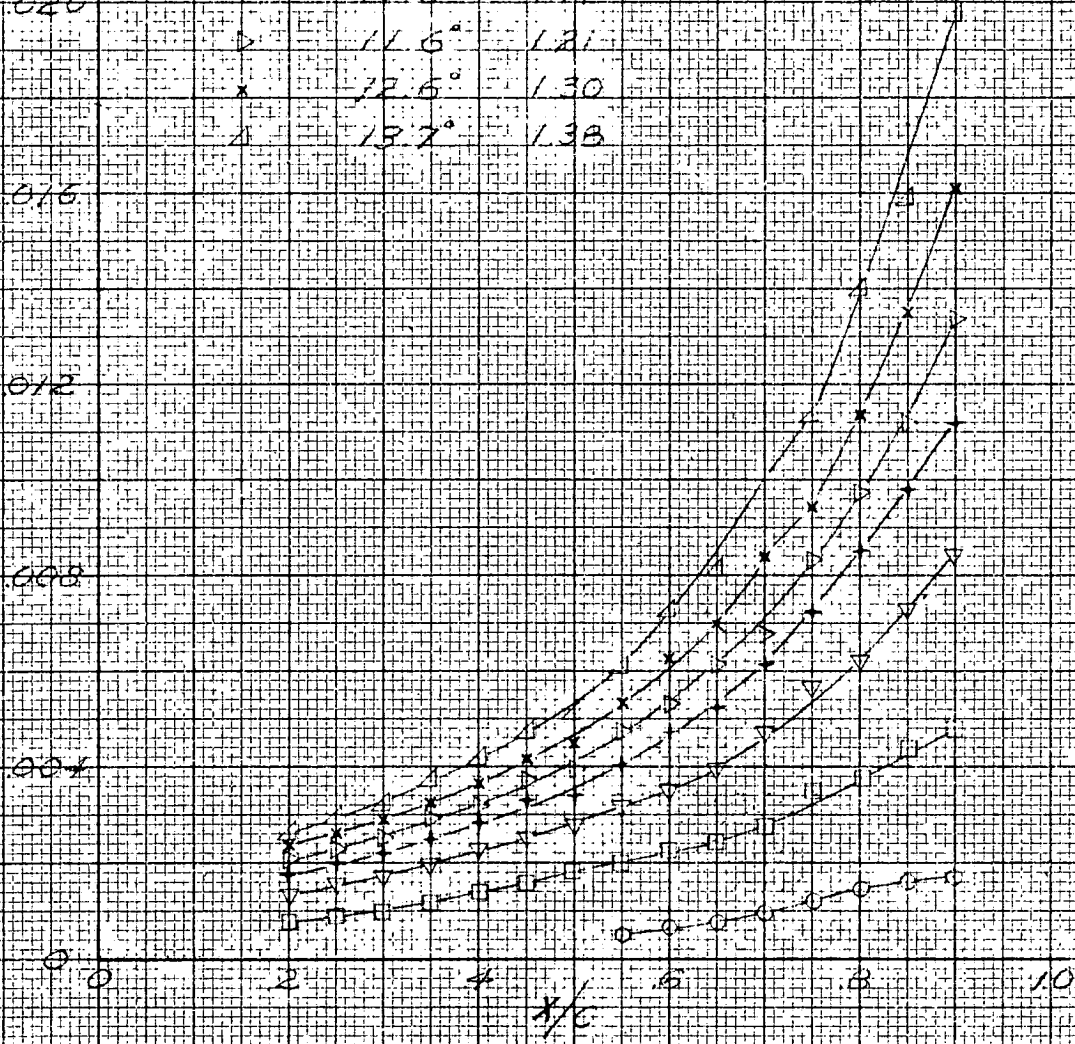
o. SPLIT FLAP DEFLECTED 40°

FIGURE 14 - CONCLUDED

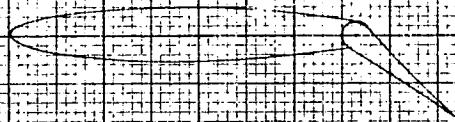


DISPLACEMENT FLOW COEFFICIENT, C_{D6}^*

α	C_{D6}^*
0	0.01
4.2°	0.45
8.4°	0.90
10.5°	1.11
11.6°	1.21
12.6°	1.30
13.7°	1.38



(a) PLAIN FLAP UNSELECTED
 FIGURE 15 - VARIATION OF THE DISPLACEMENT FLOW COEFFICIENT ALONG THE SURFACE OF THE NACA 63-012 AIRFOIL



DISPLACEMENT FLOW COEFFICIENT, C_{D5}^*

0.20

SYMBOL

α_0

C_D

○

3°

1.43

□

4.5°

1.78

◇

6.5°

1.99

⊖

7.5°

2.02

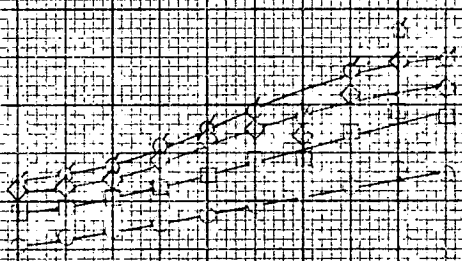
0.16

0.12

0.08

0.04

0 2 4 6 8 10
X/C



(b) PLAIN FLAP DEFLECTED 40°

FIGURE 15 - CONTINUED



DISPLACEMENT FLOW COEFFICIENT - C_{d5}

0.20
0.16
0.12
0.08
0.04
0

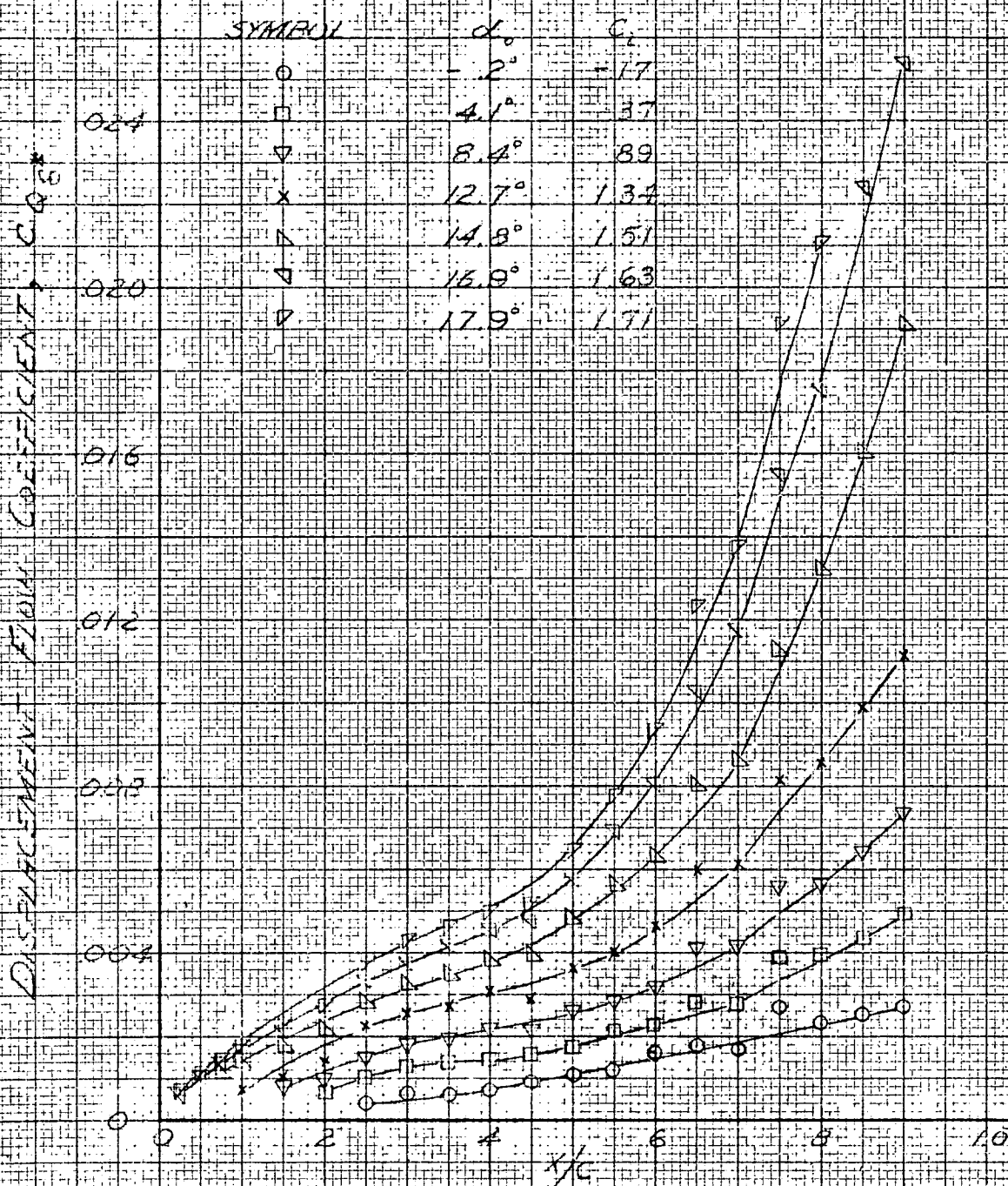
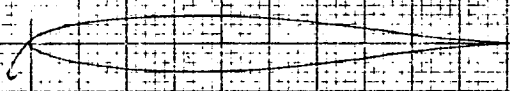
SYMBOL	α_0	C_L
○	2°	1.31
□	4.4°	1.72
△	6.5°	1.93
◇	7.6°	2.22
▽	8.6°	2.13

x/c

0 2 4 6 8 10

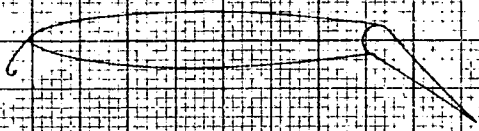
(C) SPLIT FLAP DEFLECTED 40°

FIGURE 15 - CONTINUED



(d) NOSE FLAP DEFLECTED 105°

FIGURE 15 - CONTINUED



DISPLACEMENT FLOW COEFFICIENT, C_p

SYMBOL	α_0	C_p
O	2°	1.39
E	4.5°	1.77
V	8.7°	2.12
X	13.0°	2.41
A	15.0°	2.35

0.24
0.20
0.16
0.12
0.08
0.04
0

0 2 4 x/c 6 8 10

(C) ACISE FLAP DEFLECTED 105°; PLAIN FLAP DEFLECTED 40°

FIGURE 15 - CONCLUDED.

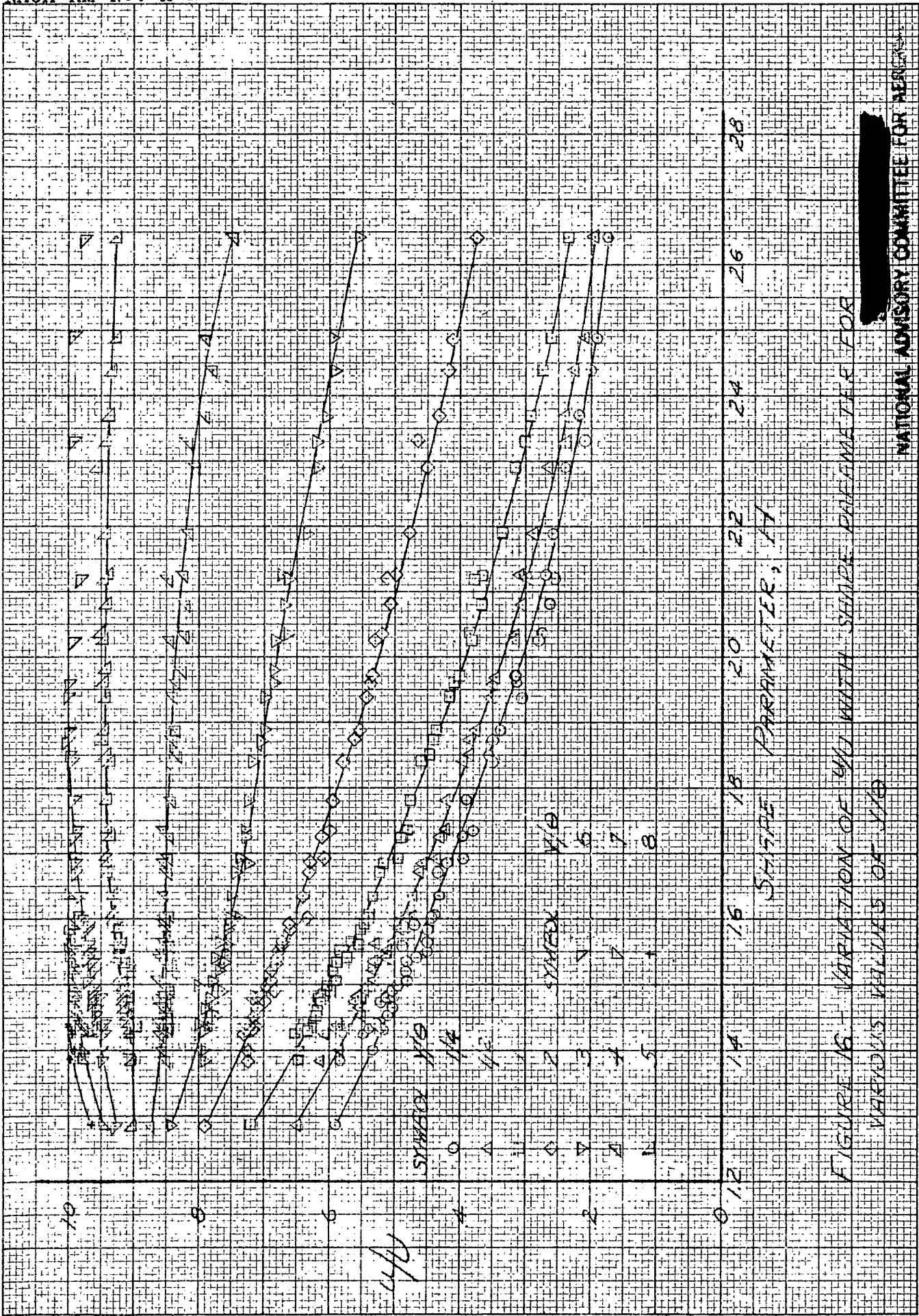


FIGURE 15. VARIATION OF y_{11} WITH SHAPE PARAMETER A FOR VARIOUS VALUES OF y_{10}

PRESENT INVESTIGATION

REFERENCE 2

REFERENCE 3

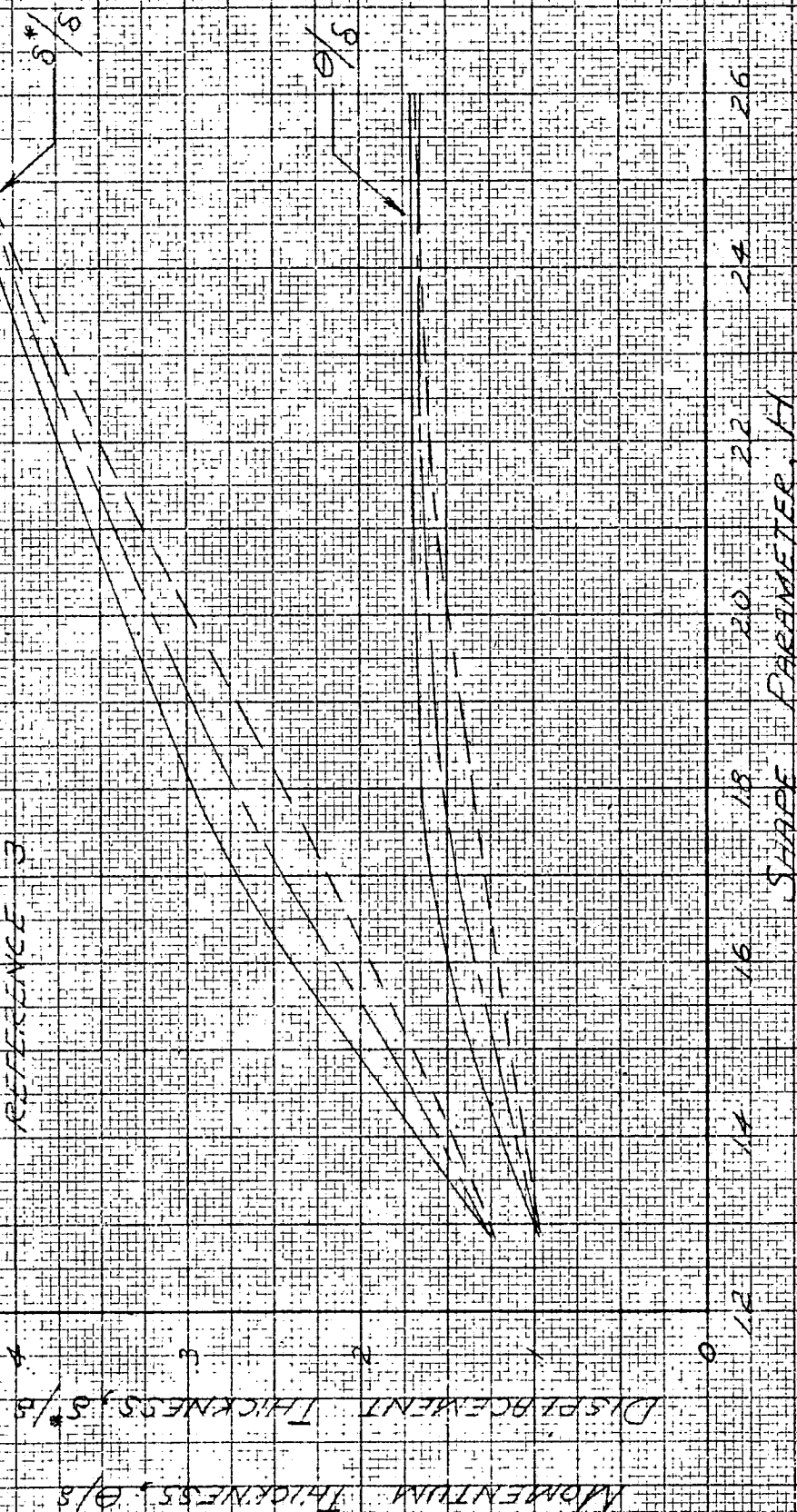


FIGURE 17 - COMPARISON OF THE VARIATIONS OF δ^*/s AND θ/s WITH SHAPE PARAMETER.

